UNIVERSITY OF COPENHAGEN

Master of Science in Geophysics

The role of oceanic signals due to D/O oscillations in the time scale of interhemispheric coupling

Maliha Shfagat Khan

Supervisor: Markus Jochum, Co-supervisor: Guido Vettoretti, Co-supervisor: Roman Nuterman

August 2021

ABSTRACT

This study aimed to a) distinguish between the relevant processes leading to abrupt warming events in the Northern hemisphere (NH), and b) to determine how heat enters the Southern Ocean and continues toward the Antarctica. Unlike many other models, the Community Earth System Model version 1 (CESM1) reconstructs self-sustained DO and AIM events. The outputs from its Last Glacial Maximum (LGM) experiment are applied to solve the climate mystery. For part a, the stochastic processes and the internal variability in the ocean were analyzed. The atmospheric stochastic processes e.g. the North Atlantic oscillations (NAO) and the wind-stress changes at several sites in the Atlantic Ocean showed to not have any influence on the break-up of sea ice in the NH. However, an oceanic dominance was detected with the temperature and salinity as the main drivers for leading the climate transitions in the NH. In part b, a description of how the heat which is originated in the DO cycles travels southward and causes the AIM is presented. We discovered that the ocean signal, which travels to the South Atlantic (SA) and Southern Ocean (SO), undergoes intermediate time scales and the in-depth southern-most signal has triangular shapes. Our research of the underlying mechanisms was inspired by Pedro et. al. (2018) [15], we found that about 2/3 of the global meridional ocean heat transport (MOHT) crosses the ACC via eddy fluxes. The eddy compartments of the MOHT have differed but the surface air temperature and ocean temperature rises to match the order of magnitude. The mystery gave rise to look for heat-pathways elsewhere for the southward travelling warm signal. The southeast tilt of the barotropic stream function (BSF) along with the large gyres in the SO are proposed to play an important role in both capturing the heat from the northern edge of the ACC and to circulate and redistribute the heat to the entire SO and to Antarctica.

CONTENTS

LIST OF FIGURES

LIST OF TABLES

Part I

INTRODUCTION

1

DANSGAARD-OESCHGER OSCILLATIONS

The dynamical nature of the earth's climate system has long been a hot topic for climate scientists from various fields. The Dansgaard-Oeschger (DO) oscillations are among the most prominent climate events of the last ice age along with its counterparts Antarctic Isotope Maxima (AIM) [11]. The term *DO oscillations* is rather misleading since the transitions between the two modes were largely random, rather than being cyclic. The DO events are abrupt transitions between the cold intervals (stadials) and relatively mild intervals (interstadials); the amplitude of the temperature variations with rapid increases followed by slow, gradual temperature falls shows a tendency toward a saw-tooth shape [18]. The oxygen isotope ratios of Δ^{18}O in Greenland ice cores are often used as proxy data for the past temperature changes, which has been shown to vary with $8-16$ °C between the stadials and interstadials. The Greenland temperature profiles during the last ice age are often mentioned by their saw-tooth appearance, as the temperatures increased relatively quickly within a few decades, while the following temperature falls took place over centuries. The counterparts AIM were more gradual and varied with $1-3$ °C [15]. Fig. 1 shows the Greenland temperature profile based on Δ^{18}O in ice cores from NGRIP (North Greenland Ice Core Project) in panel a), and the temperature profile for the AIM, which is reconstructed by the use of several ice cores from different sites in Antarctica, in panel b). Many studies have been developed in attempt to describe what triggered these interhemispheric climate transitions and how the climate of the two hemispheres connects to one another. The general consensus is that DO-events are linked to regime shifts in Atlantic Meridional Overturning Circulation

(AMOC) which provides a net heat transport from low to high latitudes in the North. AMOC transport water masses from the South to the North near the surface and returns them southward in the deep ocean [1]. However, this consensus was developed as heuristically connecting the timing and shape of the DO and AIM events with a theory on ocean heat transport and observations of palaeocean circulation [15]. The pursue of linking the abrupt climate changes to the meridional overturning circulation (MOC) i.e a variability in the MOC strengths came from the idea based upon a ocean box model of the thermohaline circulation (THC) which was proposed to be applicable to the heat transport of the Atlantic Ocean ([21]). Ocean signals are transmitted via advection, wave propagation and diffusion. Based on Stocker and Johnsen's hypothesis, the heat reservoir (the site where heat builds up) is the Southern Ocean (SO) [15], [20].

Recent studies also points toward that these climate transitions could have have been unforced and spontaneous - in other words, they occurs without any forcing and may be due to noise-induced oscillations within the coupled atmosphere-ice-ocean system [11] or internal variabilities in the oceans due to freshwater forcing and nonlinear salt oscillation which alters the ocean densities and thereby the dynamics [23].

Despite that many studies have been made, yet, it is a challenge to prove what triggers what in the combined earth system and thereby distinguish between the cause and consequences. However, more advanced climate models have been developed with better resolution and increased speed, as well as the inclusion of reservoirs which were not included in the old, simple, ideal global climate model systems. Recent models such as the Community Earth System Model (CESM), which is used throughout this study, does for example entail sea-ice and bio-geochemistry. Bio-geochemistry is not so important for this research but sea-ice and possible links to bio-geochemistry in the ocean could in perhaps alter some of the dynamics which is not fully understood yet.

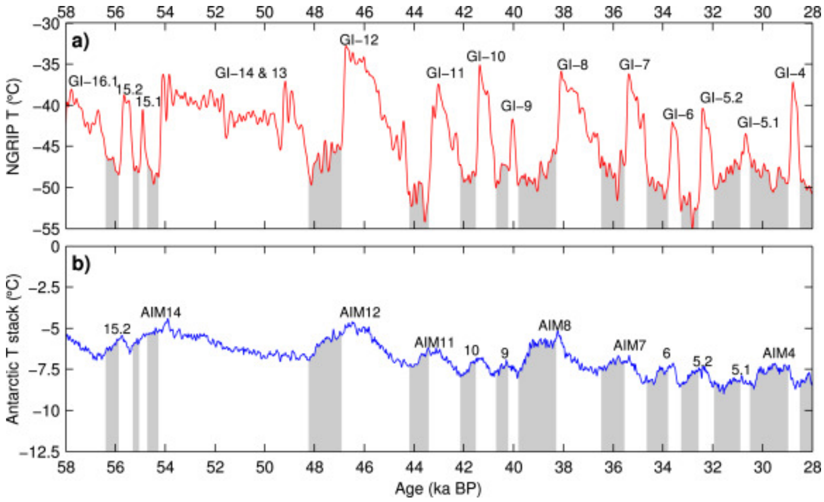

Figure 1: Adapted from [15]. Surface air temperature reconstructions based upon the temperature proxy observations of ($\delta^{18}O$, $\delta^{15}N$ and δD) concentrations in ice cores from Greenland in panel a) and Antarctica spanning Marine Isotope Stage 3 in panel b). The Greenland ice cores are from North Greenland Ice Core Project (NGRIP). The Antarctica ice cores are from six different sites: EPICA Dome C, EPICA Dronning Maud Land (EDML), Vostok, Talos Dome, and Dome Fuji. NB the DO-events are here termed as Greenland Interstadials (GI), Greenland Stadials as GS and their numbering follows Rasmussen et. al. 2014 ([17]).

1.0.1 *The pursuit of understanding the millennial scale climate changes*

The THC in the North Atlantic (NA) is a northward density driven current that transports warm salty surface water from the equatorial regions to the high latitudes. As the surface water reaches the high latitudes it undergoes a cooling, and the density increases which results in the salty water from the equator to sink. It initiates the North Atlantic Deep Water (NADW) formation in the Labrador and Greenland-Iceland-Norwegian seas. In today's climate, NADW formation occurs in the Nordic Seas and in the NA subpolar gyre (SPG) region [19]. The exact location of the NADW formation during the glacial is proposed by many studies: there are evidence for that deep water formed in the SPG during the Last Glacial Maximum (LGM), while other studies have also proposed that it was formed in the NA, or in the Norwegian Sea [19]. However, the NADW flows southwards along the west coasts of the American continent towards the SO. Mixing with other ocean basins occur while it is transported southward where it slowly warms and upwells, these small-scale processes play an important role in the NADW circulation [8]. When the MOC changes its strength, the net gain of heat is modified as well. A strong MOC gives more northward heat transport in the ocean so that the northern high-latitudes gain more heat, and the temperatures becomes high, meanwhile the opposite (a weak circulation) will result in less northward heat transport and thereby cool the regions in the northern high-latitudes. Stommel's theory from 1961 was purely density-driven i.e. alterations in salt and heat inputs [21]. Despite the simplicity of Stommel's theory it made the foundation for future development of the theory on how heat is distributed between the two hemispheres. In 1985, Broecker and his team made a further contribution in an attempt to build up a theory that explains the DO oscillations [22] [3]. According to Broecker's theory; AMOC is the key variable causing regional climate changes. As the new glacial evolved, the NA was drained from fresh water due to the buildup of ice sheets along with a southward shift of the intertropical convergence zone (ITCZ). As the Northern Hemisphere climate cools the salinification increases in the subtropical NA. This drives the system into interstadial conditions where a resultant net negative surface buoyancy flux is applied all over the high latitude NA. Even though the NA receives large amounts of freshwater fluxes via the world's river runoff, evaporation exceeds precipitation, and this causes the resulting negative surface buoyancy flux mentioned in the region. This process reactivates the NADW formation as the saltier water can sink down to greater depths. In the other climate mode, during the deglaciation period, the ITCZ shifts toward the north, and this results in a resultant net positive surface buoyancy flux all over the region of NADW formation which drives the climate into the stadial mode. Now precipitation exceeds evaporation. When the deglaciation took place (when the climate underwent a transition from the stadial to the interstadial mode), the subtropical part of NA freshened via the melt water input from land ice sheets and increased precipitation [22]. This mechanism prescribed is commonly referred to as a *salt oscillator* where salinity changes are linked to sea-ice retreat and growth. It is commonly described as self-sustained ocean circulation variability which occurs due to deviations in salt balance by sea-ice growth or retreat, a shift in the ITCZ which altered precipitation and evaporation patterns, and the greenhouse gasses. Broecker's explanation of AMOC as the main contributor is not perfect, yet it still prevailed as one of the main causes for the DO-events because it captures most of the physics and the changes seen across the broad spatial domain [11]. These types of climatic transitions were especially prominent during the Marine Isotope Stage 3 (MIS3), which occurred in the period 57-29 ka BP. The ice sheet coverage varied a lot during the last ice-age due to altering trends and extreme climatic transitions. The ice sheets had their largest extent during the LGM 21 ka years ago.

1.0.2 *Was there a stochastic trigger or did the millennial-scale climate underwent changes due to internal variability?*

The ocean circulations are maintained by a range of mechanisms such as the processes operating on the atmospheric winds, surface heat exchange, and the freshwater balance, with the presence of sea-ice influencing all these factors [11]. In the region of the SPG, strong winds meet the southernmost extension of sea ice. Through the coupling to deep ocean ventilation and overturning, SPG is hypothesized to be a dominant source of climate change trigger [11]. In a present-day climate, the SPG is a major contributor to transporting heat and salinity in the NA Ocean which further provides saline water to the Labrador Sea. Furthermore, the undergoing changes in SPG may have had a large impact on ocean deep convection and deep mixing processes - as vertical ocean processes favor strong SPG (and hereof enhances the formation of deep water). On the other side, the weak SPG circulation may result in a freshening of the NA and less deep convection (and thereby less NADW formation) [19]. In a 2015 study by Kleppin et. al., the contributors of the study suggested that the climate transitions are triggered by stochastic changes in sea level pressure patterns over the NA [10]. According to Kleppin et. al.'s research, a low pressure system over Iceland would trigger a DO-event i.e. an abrupt transition from stadial to interstadial. Pressure changes over Iceland and the Azores mimic the changes in the winds of the westerlies, air-sea buoyancy fluxes, and surface ocean properties [10].

In the first part of this research, there is a high focus on the leads and lags in the transitions from Greenland stadial (GS) to Greenland interstadial (GI). Output data from the LGM experiment made in Community Earth System Model (CESM) are used to answer the main questions. The description of the model is presented in Chapter 3. Several parameters from the model outputs are covered in this study as the main concern is to distinguish between whether the atmospheric stochastic forcing or the internal variability in the ocean triggered the climate transitions. The question of ”which role did the sea ice had during the undergoing climate changes?” is also taken into consideration. The North Atlantic oscillation (NAO) is in this study defined as the sea-level pressure changes: $NAO = P_{Iceland} - P_{Azores}$ and it is one of the parameters that we look in order to detect wind-caused climate changes. AMOC strength and SPG circulation are among the other key variables considered. Both variables draw changes on time-scales of decades or/and centuries. SPG is both sensitive to wind and buoyancy changes. Furthermore, buoyancy also affects the deep-water formation sites in the NA where AMOC is operating, therefore it also affects the strength of AMOC. The relative timings of all of these variables reveal the sequences of changes that are either leading, lagging or in-phase with the DO onsets. In the end, the result exposes whether the sea ice breaks due to stochastic forcing or due to heat transferred into the area through the dynamics of the oceans i.e. internal variability.

2

THE CROSS-HEMISPHERE SIGNAL

The bipolar seesaw mechanism has been proposed in an attempt to draw links between the DO cycles and the AIM. The bipolar seesaw mechanism is opposing "heat patterns" between the two hemispheres. The observed average time-lag between DO cycles and AIMs is 208 ± 96 years [14], [15]. The explanation of the bipolar seesaw is that the millennial oscillations are a consequence of the heat exchange between the northern and the southern hemisphere which is transported via the Atlantic Ocean. The main driver in the bipolar seesaw mechanism is the AMOC which is responsible for transferring net northward heat at all latitudes. To complete the circulation, it has as southward return flow in the deep ocean. However, the AMOC dynamics differs from the typical patterns of heat transport, which are observed in most oceans today, with the excess heat in the tropical regions tending toward the cold polar regions. The Indian and the Pacific Ocean acts according to this typical dynamic, however, the Atlantic Ocean does not do that. Therefore the Atlantic basin is the "medium" that connects the South to the North Pole. The term "conveyor belt" is often used when the cross-equatorial transport of heat in the Atlantic Ocean is explained. A very simplified explanation is a strong AMOC would warm the NA but cool the SO, likewise, a weak AMOC would cool the NA and warm the SO as more heat will be stored in the low-latitudes. Paleoclimate records have also been used to determine how ocean temperature profiles have varied when AMOC underwent changes. A warming of at least 4.6°C was detected in a sediment record of foraminiferal Mg/Ca from the Brazil Current region, this observation reveals a huge accumulation of heat in the tropical South Atlantic (SA) took place during the *Heinrich Stadial-I*[1] approximately 16ka ago [13]. Geochemist Wally Broecker proposed that freshwater fluxes and iceberg discharges could alter the AMOC as the low salinity levels at the sea surface in the Atlantic reduces the formation of deep water and the amount of heat transported northward [2]. Simple ocean model experiments of freshwater discharges into the idealized Atlantic basin do show an impact on the deep-water formation and altered surface heat patterns but more advanced and detailed models indicate weaker effects or none. Amongst many, one of the weaknesses of Broecker's explanation is it disregards the fact that the surface oceans are largely driven by winds, and it fails to explain the Heinrich events which were massive ice-rafting events that only occurred under the very cold conditions both before and during these events.

This study is partly based on "the beyond the bipolar seesaw" experiments done by Joel Pedro and colleagues [15]. Pedro's study uses a coupled earth system model with two different experimental setups for freshwater fluxes that alters the stadial-interstadial transitions. Some of the key findings to be mentioned from Pedro's study [15]:

- After the AMOC collapses, heat accumulates in all oceans north of the Antarctic circumpolar current (ACC) and not foremost in the SA and the SO as earlier theories for bipolar seesaw suggested. In this view, the global ocean act as a heat reservoir and not solely the SO as first proposed by Stocker and Johnsen [20].

- Examinations of energy budgets, specifically, the meridional energy components showed that heat fluxes enter the Antarctic continent via a complex combination of eddy advection, diffusion, sea ice retreat, and changes in the air-sea heat flux. The combination of these processes are responsible for transferring the signal into Antarctica.

1 Heinrich events refer to the occurrence in NA oceanic sediments of layers of ice-rafted debris (IRD), and are thought to be due to a massive discharge of icebergs from the Laurentide ice sheet, and particularly from the ice stream in Hudson Strait, which drained the Hudson Bay ice dome (since the lithic fragments of the IRD largely come from there). From: Encyclopedia of Atmospheric Sciences, 2003

Other studies with climate models have also shown the phenomenon described above, which was that when the NA cools in these cold glacial environments, heat accumulates in the tropical and mid-latitude Atlantic [23]. The ACC acts as a barrier that is flowing in circular paths around Antarctica, the absence of continents, and the presence of strong westerly winds makes it the largest ocean current with high speeds between 100-150 Sv or even faster [6]. Ocean waves can not pass across ACC therefore one will have to look for the impacts from elsewhere such as in the mean flow, oceanic eddies and diffusion. However, even small amounts of heat are sufficient to initiate warming in the SO and melt the sea ice. Heat can be spread throughout the ocean across ACC via eddies or break-up of waves due to chaotic dynamics. There are several hotspots where heat can pass through the ACC via the eddies, an example is near the Drake Passage. Other processes than eddy fluxes may also be looked in details. CESM1 is well-resolved in the SO, the SH can thereby be studied in details, and the model provides a ”detailed” overview of the interplay between sea-ice, the large gyre circulations, the alterations in albedo, and changes imposed into or by the atmosphere - as eddies are both gaining energy input from the atmosphere and ocean forcing. In addition to the large gyres which are mentioned extraordinarily in this study, the influence of the large gyres in the SO is also looked up in detail. Oceanic heat transport from eddies can explain some of the influxes of heat but the ocean gyres are much faster moving circulating current which could in principle capture heat near the ACC front, circulate, and redistribute it all over the SO. This is one of the mechanisms which is hypothesized to make up the so-called ”heat pathways” toward Antarctica. The study by Laurits S. Andreasen and team (see A.1) is a further investigation of the ocean connection between Greenland and Antarctica. Andreasen tested the slowest mechanism responsible for the heat propagation from the SA into the SO in a simple ocean-only model called VEROS [2]. Andreasen's study suggested a mathematical model describing the time-lag in the adjustment processes in the SA and in the SO whereof it appeared that adiabatic and geostrophic processes are dominant in the SA while eddy advection appeared as the most dominant process in the SO and thereby the main mechanism for carry

2 VEROS, the versatile ocean simulator, a purely python based model [9].

energy across the ACC (see fig. 6 in A.1). The LGM experiment in CESM1 provided different outputs for the energies, the meridional ocean heat transfer components reveal which dynamical mechanism is the most important at a given latitude. The energies reveal the importance of each output across ACC (and in other locations). The results for the global ocean heat transports are presented in ch. 6 where the stadial and interstadial modes are studied separately.

Part II

MODEL DESCRIPTION

3

COMMUNITY EARTH SYSTEM MODEL

The Community Earth System Model (CESM) with marine and terrestrial biogeochemistry (BGC) is configured to simulate the time-period from LGM event (21 kyr ago) to the Bølling-Allerød (BA) event (14 kyr ago). The LGM has been simulated and re-produced in several ESMs which aligns with observations. The special feature of our model is that it also entails the biogeochemical properties of the oceans which is essential for understanding how the marine carbon cycle affects the climate system. The dynamic behind the BGC of the oceans, such as the tracer concentrations of dissolved organic and inorganic carbon, is not important for the explanations of the results. The BGC will not be explained any further. The model being used here is the coarse resolution *CESM version 1.0 (CESM1)*. The spatial resolution varies with location. The ocean resolution around Greenland is approximately 20 km, while it becomes less well-resolved in other locations such as in the Southern Ocean where it is about 100 km, and around 400 km in the subtropical North Pacific. The model has 60 ocean layers with uneven thickness, the thickness varies and it is 10 m close to the surface and up to 250 m at the bottom. The ocean part of the model is composed of a subgrid-scale model for the mesoscale eddy mixing on isopycnal surfaces which was build for non-eddy-resolving ocean circulation models by Gent and McWilliams in 1990 (GM90), since its development, GM90 has been one of the most widely used models for representing the transfer properties in non-eddy-resolving on isopycnal coordinates [7]. The vertical structure of the ocean model is based upon the model built for vertical variations of thickness diffusivity by Danabasoglu and Marshall in 2007 [5]. The atmospheric model is composed of 26 vertical layers and it uses a T31 spectral truncation which is 96 by 48 regular longitude/latitude global horizontal grids cells (approximately 3.75 degree resolution). The sea-ice model shares the same horizontal grid as the ocean model and the land model is on the same horizontal grid as the atmospheric model. The CESM1 is accessible for most universities, it is both providing a realistic representation. The model uses 160 cores and takes one day to simulate 90 model years. Despite having low resolution and low cost, it is in competition with high resolution models which are 10 times more expensive one degree resolution version.

The model uses some inputs to generate the climatic conditions which were present during the time period between LGM and BA. We use a fixed surface mixing of $2 \times 10^3\ m^2\ s^{-1}$ and a fixed empirical vertical mixing profile (after Bryan-Lewis) of $0.1 \times 10^{-4}\ m^2\ s^{-1}$ in the upper ocean [4]. The overflow parameterization was removed. The ice sheet orography and bathymetry are based on model reconstruction by Peltier (2015) [16]. The orbital forcing parameters for insolation are those corresponding to 21 kya, the insulation levels during this period were close to those in present day [18]. The climatic variability is not forced or triggered by modulating any of the variables involved in the model setup. To first order, the DO-oscillations are salt oscillations. During the cold stadials, the seawater temperatures at most sites are close to the freezing point. Therefore, the density variations over the whole water columns are mainly due to salinity since changes in water temperature isn't making any huge impacts on the densities.

The temperature variations in our model are the result of a self-sustained nonlinear oscillation of the coupled atmosphere-ocean-sea ice system. It is a coupled process involving temperature and the hydrological cycle also with coupling in the ocean-atmosphere and sea-ice (and land because of rivers), so thereby the whole Earth. Therefore, one may also call them hydro-thermohaline oscillations.

Part III

RESULTS

4

STOCHASTIC ATMOSPHERE FORCING VS OCEANIC OSCILLATOR

The modelled LGM temperature profiles shows the specific feature of the DO cycles (see green surface temperature time-series in Fig. 2) where the long cycles appear with a two step cooling process that resembles a sawtooth (see fig. 1 where temperature observations for the ice core sites at NGRIP and Antarctica are presented). The Greenland interstadial onsets occurred at model-year 4390 and then again at model-year 5480. The stadial onsets are also marked in Fig. 2.

The onsets marked in Fig. 2 are used in all of the later results in an attempt to distinguish between the dynamical processes and to make a further investigation of what happens during the time periods around the Greenland stadials and Greenland interstadials, respectively.

A set of subplots of different variables are visualised in fig. 3 over the time period running over two DO cycles, the presented variables are from the top: AMOC strength variability measured in sverdrup (Sv); sea ice fraction in the southern region of Iceland; NAO variability measured as the sea surface pressure differences between the sites Iceland and Azores; the upper 500 m sea temperature changes in the Southern Ocean; and the variability of the subpolar gyre strength. There was a significant high accumulation of sea ice in the Arctic Ocean during cold stadial condition (second subplot from top in Fig. 3). The most prominent and conspicuous sea ice changes occurred in the region South of Iceland, the region did appear as the most sensitive toward climatic changes in the northern hemisphere in the modelled LGM (green curve in Fig. 3). A fourth part of the ice fraction disappears during the DO onsets from from 72% to 47%. The last subplot (olive curve) in fig. 3 shows the strength of

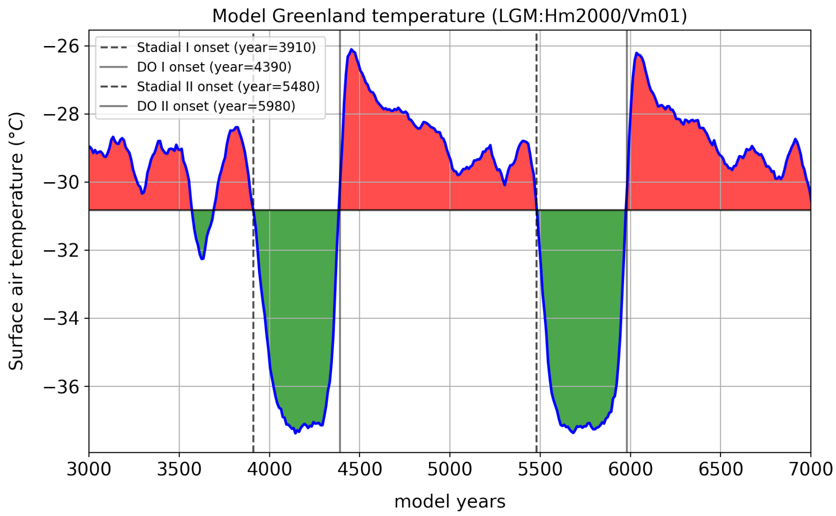

Figure 2: Reconstruction of the average Greenland surface air temperatures during initial conditions that corresponds to the time-period between LGM and BA event. The average temperature over the whole period is $-34.67\,^{\circ}\,C$, the temperatures below (marked with green) this threshold defines the stadials while the temperature above (red) are the interstadials. The vertical lines mark the onsets of stadial and interstadial onsets, these times are used for the study of the environmental changes during glacial and interglacial respectively.

the subpolar gyre. Changes in SPG strength are dependent on changes in wind patterns, which have been postulated via earlier studies, to be important for the setting the ocean circulations in the upper ocean [11]. The results presented in fig. 3 are with no doubt showing an oceanic dominance, the SO temperatures (in the purple curve in fig. 3) increase much earlier than any of the other variables presented prior to the DO events, the SPG strength increase in amplitude toward a larger negative value prior to the increase of AMOC strength. As the NH climate is switched toward the interstadial (DO onsets) mode, the strength weakens from -14Sv to -9Sv. A strong SPG circulation is associated with deep water formation in the region. The AMOC strengths are essential for how much heat is transported across the NA and toward the polar regions. From the results presented in the green curve (fig. 3) it can be argued that a large portion of sea-ice in the surrounding ocean in the southern part of Iceland disappears within a few years after AMOC intensifies its heat transport. The contribution from the winds are not so obvious as they are not causing large impacts pushing toward a glaciation, the North Atlantic oscillation (NAO) index (red curve in fig. 3) appears as highly variable during the interstadial but its oscillating appearance is strongly weakened during the stadial where ice dominates the landscapes and oceans. Wind patterns across the Atlantic Ocean are not so important for initiating

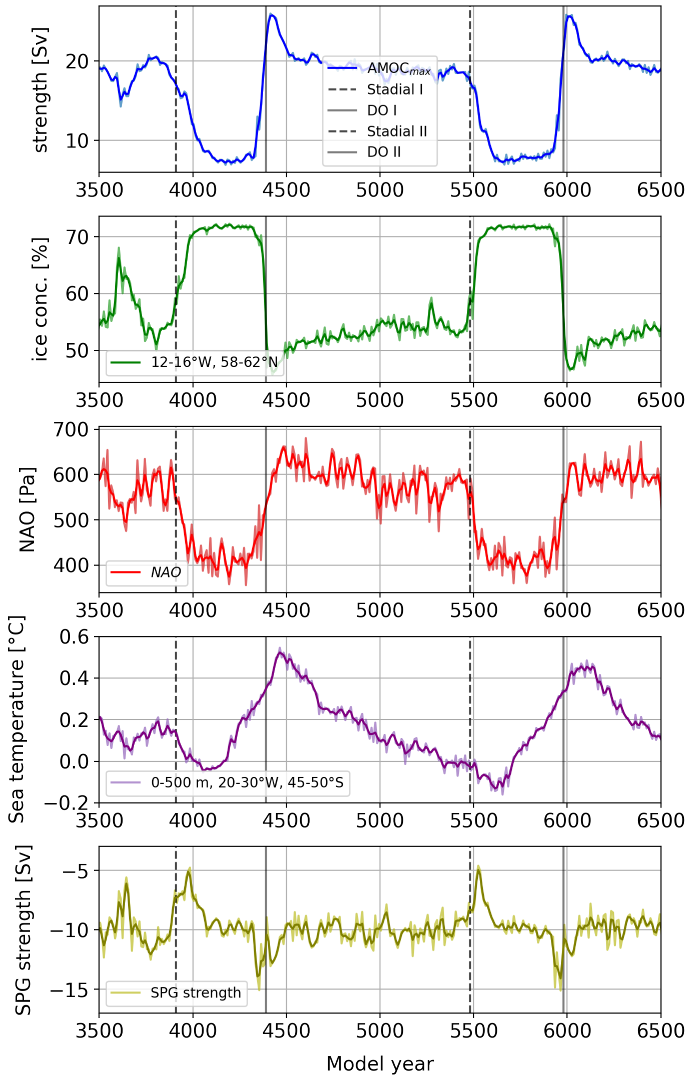

Figure 3: Modelled variables in a LGM configuration. The grey vertical line (year 4390) marks the onset of the Greenland interstadial. From top: variability of AMOC strength; sea-ice concentration in the ocean region in the southern parts of Iceland; variability of NAO in terms of pressure differences between Iceland and Azores; average ocean temperature of the upper 500 m of the Southern Ocean; and the strength of the Subpolar gyre.

a glaciation (red (ice fraction) and green (NAO) curves in fig. 3). However, the key finding is that the atmospheric pressure is not leading to the breakup of the sea ice and the same applies for the wind stress over the Atlantic (figure 4. The sea ice variability happens due to changes in gyre circulation or

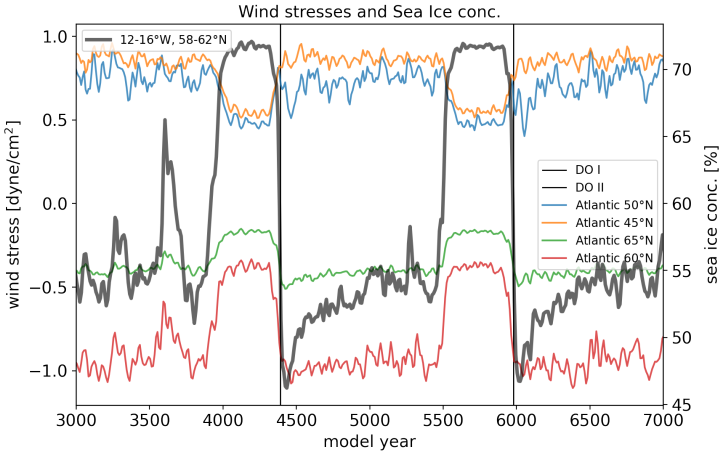

Figure 4: Sea ice concentration in the ocean surrounding the southern part of Iceland (thick grey line), and wind-stresses over the Atlantic Ocean and the Atlantic section of Southern Ocean. The wind stresses over the North Atlantic are generally weakened during the stadial, and from these results there is no indication for that sea ice retreats due to winds.

ocean advection. The main result of the problem regarding stochastic atmosphere forcing vs oceanic oscillator is that the ocean heat transport is leading in the DO cycles. The stochastic variability of the atmosphere can not have any effect on the ocean (in a direct sense) when sea ice is present and thereby becomes responsible for breaking the sea ice in the NH. The sea ice has to be gone before stochastic processes can be prescribed any important roles. Evidences for the oceanic dominance is stronger: the depth profiles of sea temperature and salinity in different regions in the Northern hemisphere are described in the following chapter 4.1 along with how it links to the abrupt climate transitions.

4.1 DESCRIBING WHY DO-OSCILLATIONS ARE SALT-OSCILLATIONS (IN FIRST ORDER)

The climatic variability is not forced or triggered by the modulation of the variables involved in the model setup. To first order, the DO oscillations are *salt oscillations*. The ocean is an important reservoir due to its ability to both store and transport large amounts of heat and energy. Buoyancy forcing and freshwater are among others processes which controls oceanic dynamics, properties and salt content. During the cold stadial periods, the seawater temperatures at most sites were close to the freezing point, therefore, the density variations over the whole water columns are mainly due to salinity changes since changes in temperature are not making any huge impacts on the densities. The

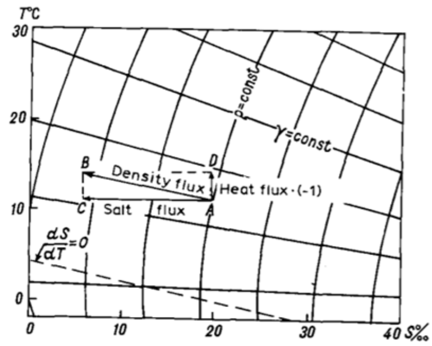

Figure 5: TS-diagram. Here the density flux, γ, depends on the isopycnic potential ρ, salinity, S, and temperature, T. The density flux can be expressed as $\gamma = \int_{T_0}^{T}(\frac{\delta\rho}{\delta S})_{S_0}dT - \int_{S_0}^{S}(\frac{\delta\rho}{\delta T})dS$. The nonlinear equation of state of sea-water is vigorous as it reveal substantial properties of the interactions and transformations of the sea waters. The density flux is often calculated numerically. The details and mathematical aspects of the density flux will not be discussed but its application to oceanography will. Figure adapted from [12].

TS-diagrams for seawater is shown in fig. 6. The diagrams present the nonlinear linkage between temperature and salinity of the water. The contour lines of constant density are nearly vertical close to zero degrees Celsius, which means that small changes in temperature, T, are not able to change the seawater density remarkably but changes in salinity are able to do this.

The nonlinear function for density ρ is diagnostically dependent on T, temperature, and S, salinity and p, pressure:

$$\rho = \rho(T, S, p) \tag{1}$$

Buoyancy forces in the ocean occur due to density differences ($-g\Delta\rho$). The explanations in this section are mainly involving the DO-I (however, the behaviours around DO-II were comparable

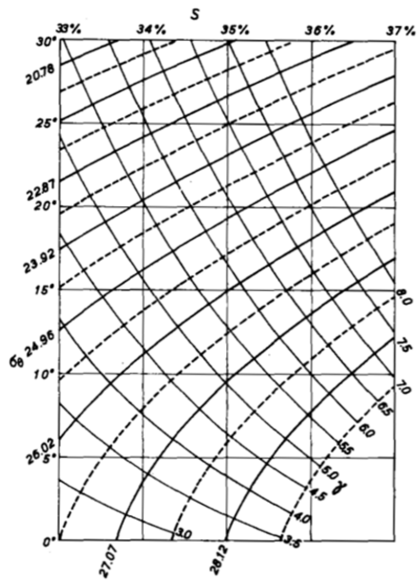

Figure 6: A numerical representation of function γ in ranges $0 \leq T \leq 30°C$ and $33 \leq S \leq 37‰$. Figure adapted from [12].

to DO-I). In the following temperature and salinity depth profiles for the regions, Nordic Seas and Irminger and Labrador Sea will be presented.

4.1.1 *Salt and temperature anomalies in Nordic Seas, and in the Labrador and Irminger Seas*

The results presented here are anomalies where the time average which are subtracted are based on means between model years 4905 and 7150. The first set of subplots shown in fig. 7 shows the temperature and salinity anomalies in the time-span between (model) year 4200-4700 in the Nordic Seas, and the next set of subplots in fig. 8 shows the same variables in the same time-span but for the Irminger and Labrador Seas. The choice of looking at the Nordic Seas is based upon the fact that the surface climate of Greenland is argued to be sensitive toward the variability of sea-ice in the Nordic Seas. The variability of sea-ice is in turn dependent on changes occurring in ocean heat transport. The reduced heat transport via the overturning circulation and the subpolar gyre are, along with other mechanisms, responsible for the ice growth in the Nordic Seas [11], [19].

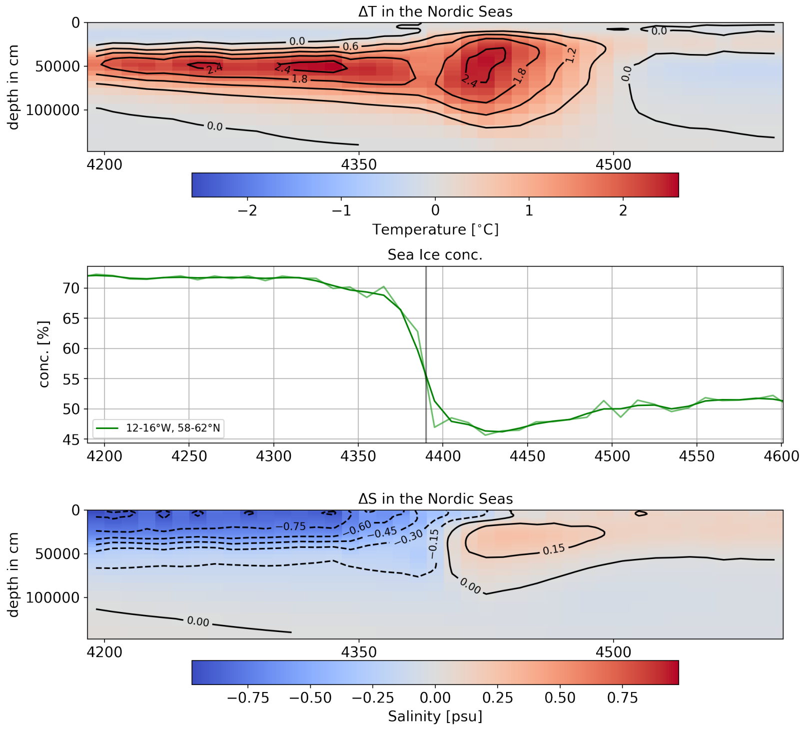

Figure 7: Variations in temperature and salinity in the Nordic Seas, and the sea ice changes in the Iceland basin along with the interstadial onset marked at year 4390. The depth vs latitude plots of the temporal changes during the cold stadial conditions in the Atlantic basin revealed that heat was being captured underneath the ice cold surface waters of NA. Furthermore, this representation reveals that those conditions a very unstable and diffusive processes will be initiated and expanding the heat in the depths, and sea-ice is forced to break-up from its bottom.

As it appears in fig. 7 prior to the Greenland interstadial onset, heat is being accumulated below the halocline in the lower edge of the sea ice. The increasing heat promotes instability and vertical mixing, and the melt of sea ice. The period before the onset of deglaciation was dominated by the LGM where the deep convection in the Nordic Seas was both weak and unstable [19]. The mechanism described above is not sufficient enough to initiate a DO cycle, DO-like dynamics can only be generated if ocean heat fluxes into the Nordic Seas are being accounted for [11]. The ocean heat transports are presented Chap. 6.

The temperature and salinity variations with depth in the Labrador and Irminger Seas are shown in fig. 8. In today's climate, Labrador and Irminger Seas are the most important regions for the North

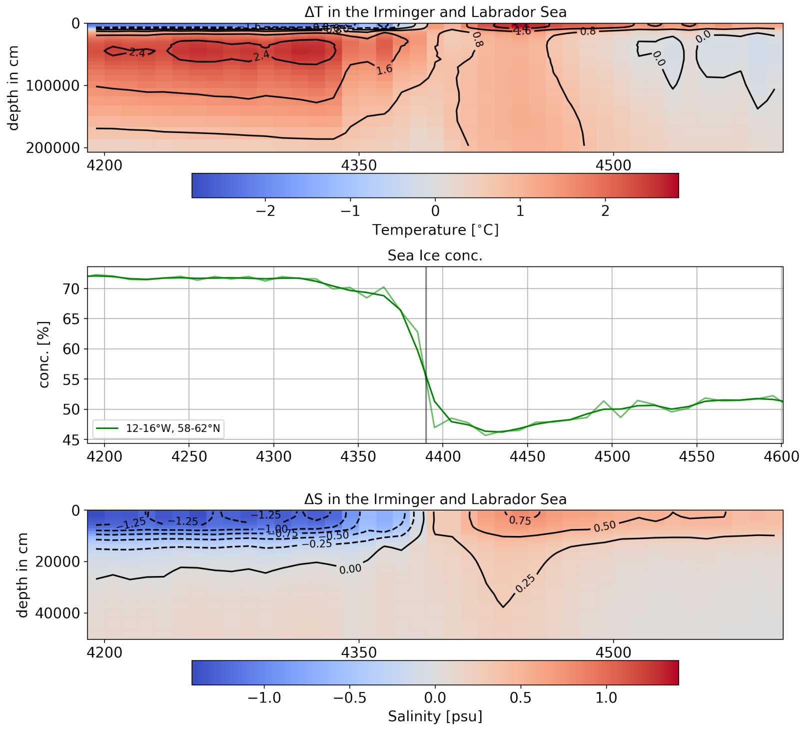

Figure 8: Temperature and salinity anomalies in the Labrador and Irminger Seas along with sea ice concentration in the Iceland basin are presented, the vertical line is marking the DO-onset at year 4390. During the cold stadial conditions, there is a temporal expansion of heat underneath the ice covered surfaces of the Irminger and Lanbrador Seas. The temporal buildup and trapping of heat explains the melting of sea ice above in the Iceland basin, the heat trap is slowly being released to the surface until the climate has fully undergone a transition into the warm interstadial period.

Atlantic deep convection but the location and strength of deep mixing during the last ice age is debated [19]. A recent study of sediment records from Labrador Sea has shown, during the very cold stadial period of LGM, the deep and surface circulation in the Labrador Sea did receive warm and saline water from the Atlantic Ocean [19].

The general patterns are that before the DO-I event (model-year 4390) happens, the surface waters are relatively fresh and contains less salt. It is due to the presence of sea ice in these regions. Both in the Nordic Seas and in the marine region around the Irminger Sea, the relative changes are happening in roughly the upper 1 km of the ocean column, the changes underneath are negligible. The marine region about the Irminger Sea and Labrador Sea is showing more interesting results, the surface layers are very thin and fresh (or even frozen), small amount of salt ¡0.5psu is being accumulated below the upper 100 m. The ocean is unstable, and heat that travels from the lower latitudes and tropics is being transported into the basins in fig. 7 and fig. 8. In the transition between the cold and the warm period, diffusive and convective processes are occurring (diffusive processes are less important than the former). As sea-ice disappears slowly due to the heat buildup within the ocean, other processes are also intensified. Warm surface currents (heated by solar radiation) from the tropics which are initiated by surface wind approach the surfaces from underneath of the ice in the high-latitude. The results from the Nordic Seas and Irminger and Labrador Sea in fig. 7 and fig. 8 support the salt-oscillation theory combined with ocean currents as internal variables. The abrupt warming of the NH is a consequence of the slow northward travelling heat from the SO (as shown in 3), the (vertical) buildup of heat and salt-content alteration (primarily in the Nordic Seas).

5

HOW THE SIGNAL GETS TO ANTARCTICA

In an attempt to connect the two hemispheres and their adjustments to the stadial and interstadial environments, the two modes are analyzed separately. Some of the key model generated climate variables during the stadial and the interstadial are presented in fig. 9. The mean modelled NGRIP temperature drops by 4 °C during the stadial and raises by 4.5 °C during the interstadial. The NGRIP temperature profiles are in phase with AMOC strength changes. The modelled EDML temperature falls and rises are gradual. During the (NH) stadial, EDML temperature falls by 2.5 °C per century and vice versa during the interstadial. There are indications for that the upper ocean water of the SO section 45-50°S, 20-30°W is in phase with the mean EDML temperatures during the interstadial period. This does not hold for the stadial mode where the SO upper ocean temperature cools by approx 0.1 °C within the first 100 years, other processes may become important in this mode in the SH as sea ice expands. The results presented in figure 9 clearly show that there is not a traditional seesaw mechanism between the northern and the southern hemisphere; heat enters the southern ocean and crosses the ACC after the first warm signal in the north polar regions is detected. Depth vs. latitude plots of temperature anomalies in the Atlantic and the Atlantic section of the Southern Ocean at different time intervals after the respective climate transition (stadial and interstadial) onsets are here used for detecting how the meridional heat distributes and how it moves at different depths. The time intervals are; $t_0 - t_{50}$ which is read as *the average between 0-50 yrs after the stadial/interstadial onset*, $t_{50} - t_{100}$, $t_{100} - t_{200}$ and $t_{200} - t_{300}$. The stadial mode is presented in fig. 10 (for the Atlantic

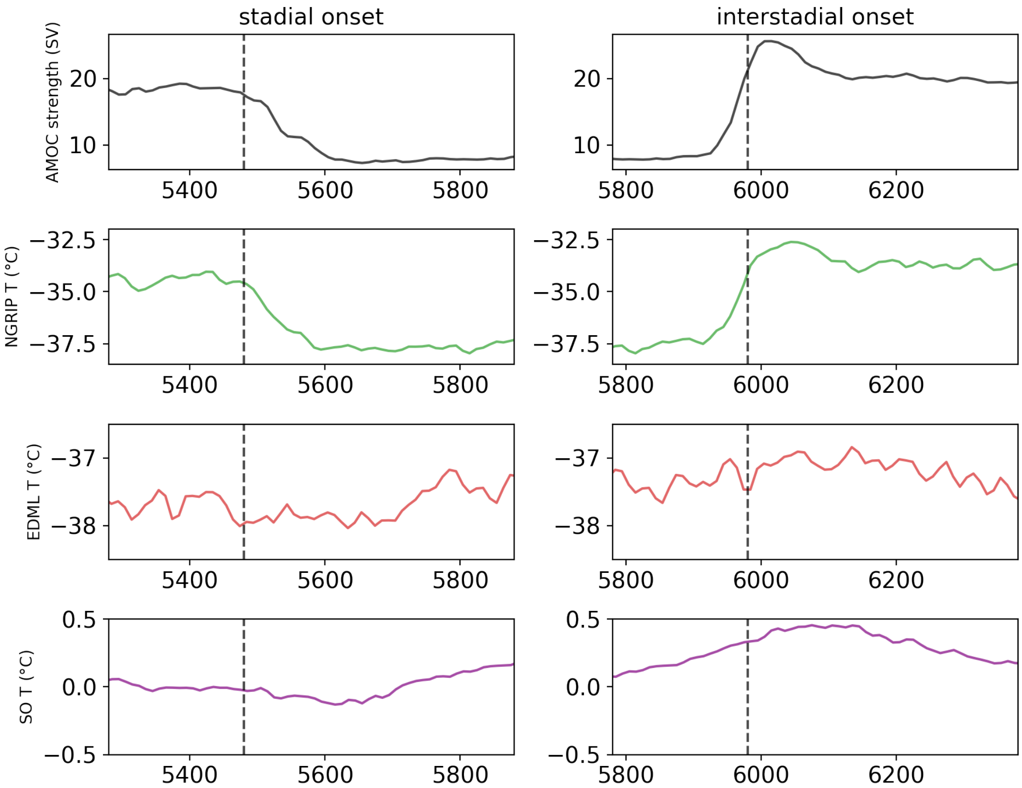

Figure 9: The time is in the x-axis. Key modelled climate variables during the stadial (left panel) and the interstadial (right panel) are presented along with AMOC changes. The dashed lines mark the stadial onset at year 5480 and the interstadial onset at year 5980 as first introduced in fig. 2. From top: AMOC strength; surface air temperature in the grid-cell corresponding to the NGRIP ice core site; surface air temperature in the grid cells corresponding to the Antarctic EDML ice core site; Southern Ocean upper ocean temperature (0-500 m depth, 45-50°S, 20-30°W). All data are 10-year means.

and the Atlantic section of the SO), fig. 11 (for the Atlantic Ocean). and fig. 12 (for the Atlantic section of the SO). The interstadial mode is presented in fig. 13 (for the Atlantic and the Atlantic section of the SO), fig. 14 (for the Atlantic Ocean) and fig. 15 (for the Atlantic section of the SO).

In the stadial mode, the Atlantic Ocean is cooled almost everywhere at the surface, both the South and the North Atlantic oceans show cooling trends in the first hundred years with the North Atlantic being cooled the most (see fig. 10 and fig. 11). Especially, during the first 50 years, we see cooling trends everywhere. In the next 50 to 100 years, heat slowly accumulates below the surface. In the northernmost part of the North Atlantic, the heat is trapped more quickly while the surface cools very

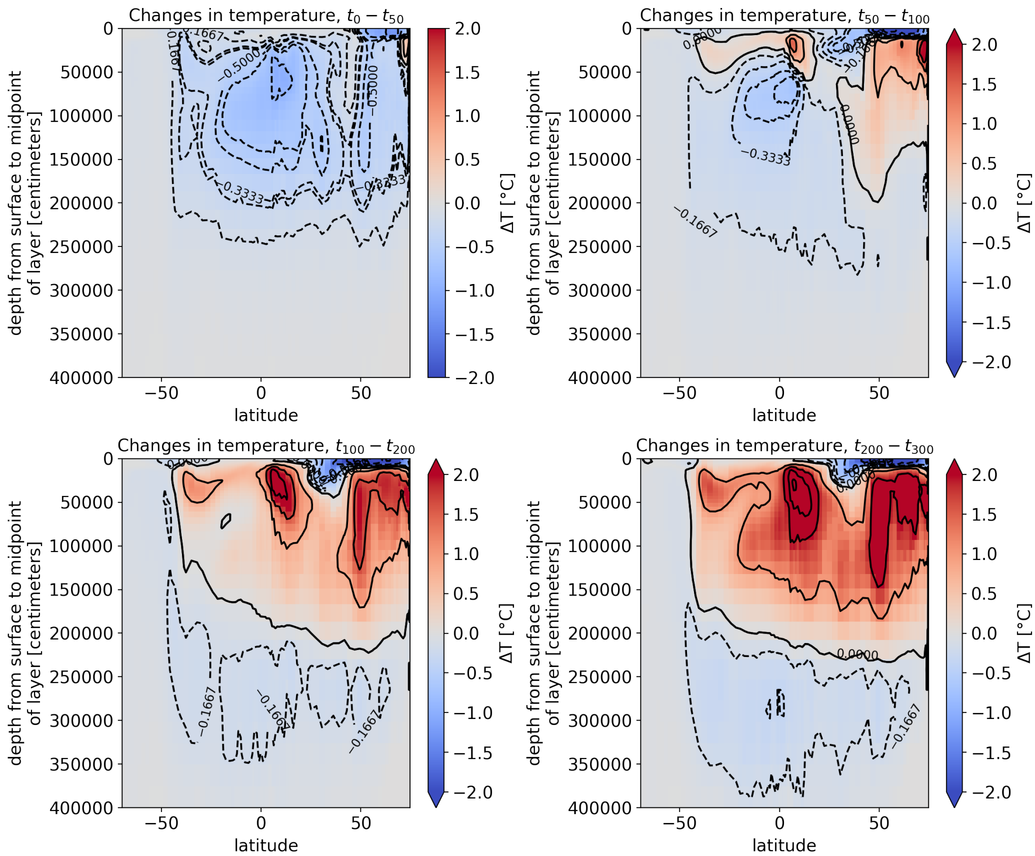

Figure 10: After stadial: temporal temperature anomaly adjustments in the Atlantic and the Atlantic section of the Southern Ocean.

fast as sea ice expands. After 100 years the contrast between the North and the South Atlantic Ocean becomes clear as the signal becomes more apparent as the North Atlantic cools more rapidly and heat is gradually being trapped in the depths of 300m and spans down to 1.5 km below the sea surface after 200-300 years. In other words, the South Atlantic thermocline deepens on a decadal-scale. The two heat cells, the one which is being built under the Arctic sea ice and the other which is accumulated in the South Atlantic, expands temporally. This is due to several dynamical processes: the built-up of sea ice in the Arctic and thereby heat is released to the ocean layers below the surface; the weakening of AMOC which is no longer transferring heat from the South to the North cause a heat trap in the subsurface ocean between 50 °S and 12°N; the thermocline deepening which allows more heat to be stored in depths. A seesaw-like pattern appears between the North and the South Atlantic, meanwhile, the strong ocean current encircling Antarctica, the ACC, makes it impossible for the heat (warm cells)

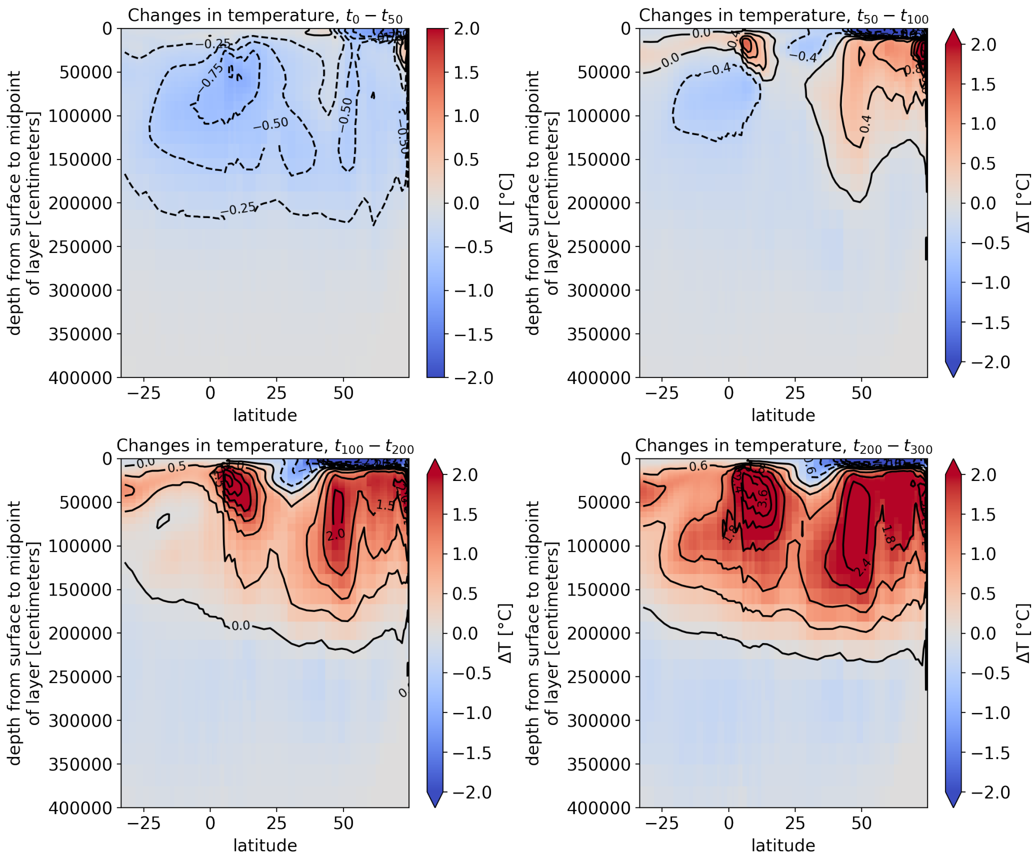

Figure 11: After stadial: temporal temperature anomaly adjustments in the Atlantic.

to enter further South. The South-North Atlantic contrast is mainly caused by the reduced northward advection (described in the following chapter, see chapter **??**), and the thermocline deepening which allows heat to accumulate in the South Atlantic. Therefore, Antarctica remains cold for a long time before it starts to react. The responses in each basins happens on intermediate time-scales, this is explained later and presented in fig. 18 and fig. 16.

There is not a one-to-one contrast between the stadial and interstadial. When the DO abrupt warming event start, positive temperature anomalies are already occurring throughout the surfaces of the entire Atlantic Ocean and the Southern Ocean (see fig. 13, fig. 14 and fig. 15). A temporal downward movement of the deep ocean is observed as the thermocline as the heat i.e the warmer layers above expands downward (see fig. 13). Unlike the study by Pedro and team (for comparison look at figure 5, 7 and 8 in [15]), the climate signals tend to be strongest and have higher amplitudes within the first 50 years afterward other dynamical processes start becoming more dominant and

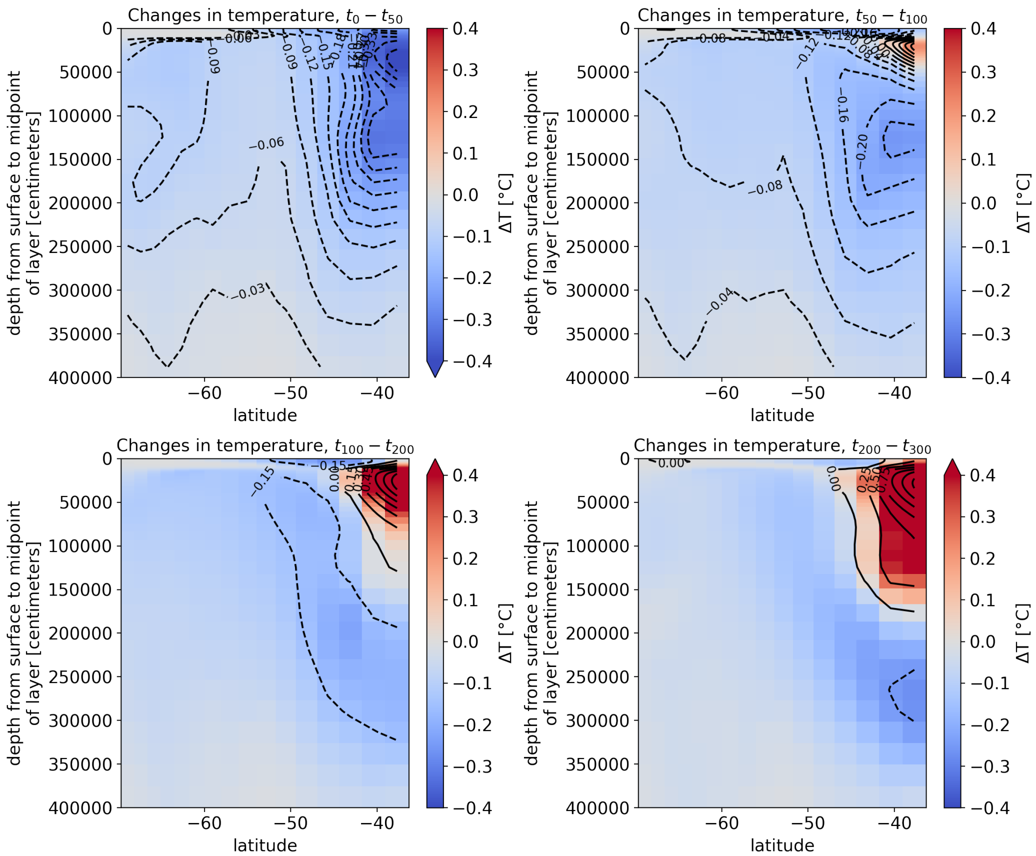

Figure 12: After stadial: temporal temperature anomaly adjustments in the Atlantic section of the Southern Ocean.

redistributes the ocean signals. In Fig. 13 and its accompanying figure 14, a strong positive ocean temperature anomaly signal is observed in the equator at 1000m depth (see upper left subplot of figure 13), this signal is temporally damped. Two cold water cells in either sides (edges) of the South Atlantic are detected in depths below the surface and above this warm cell at 1000m depth, there is a northward migration of this subsurface cold waters. The cold cells sinks gradually with time at 40 °N in the North Atlantic, and the remaining ocean is forced into an unstable environment. After examining the results for the interstadial mode, one can be tempted to argue that this indicates toward a very complex dynamics compared to the classical understanding of the AMOC as warm waters from the South is transported to the North in the interior of the Atlantic Ocean. The layers above it are colder and these are also being pushed northward in the upper layers, it is primarily observed in the first 100 years. Whenever surface water becomes denser than the underlying water, convection occurs.

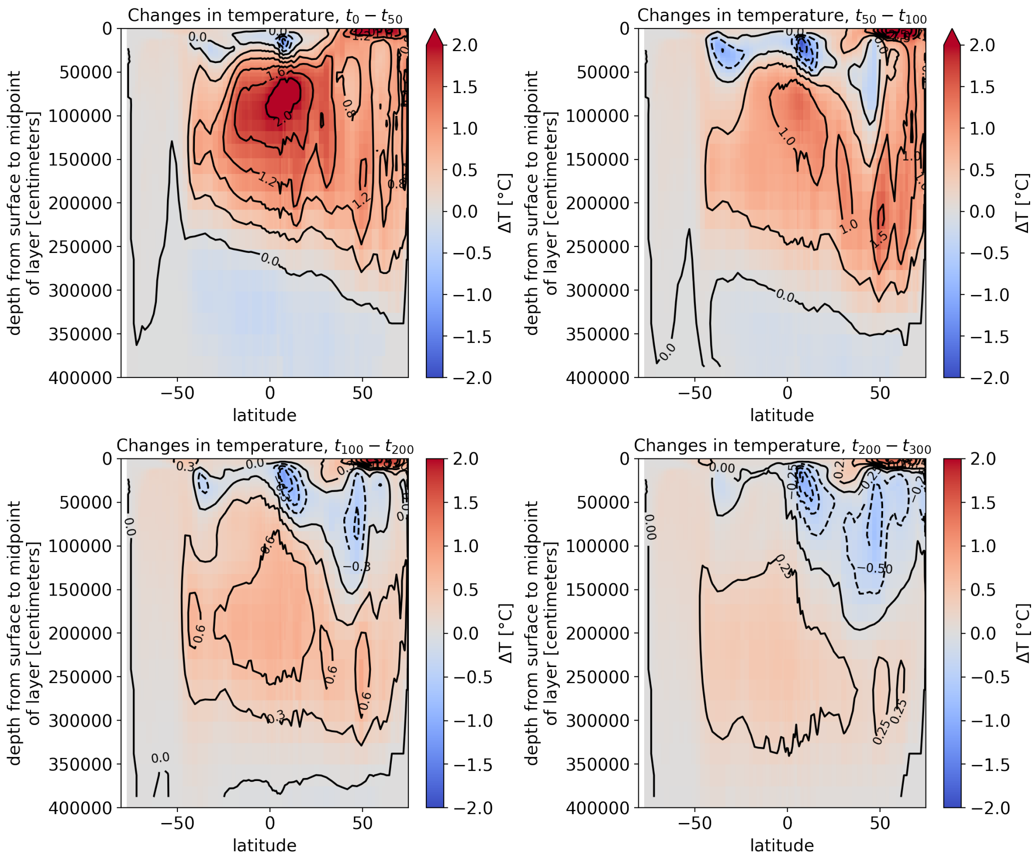

Figure 13: After interstadial: temporal temperature anomaly adjustments in the Atlantic and the Atlantic section of the Southern Ocean.

At the same one has to consider the intersection between the atmosphere and the ocean, excess heat is both being redistributed and released to the overlaying atmosphere, this is what the plots for 100-200 and 200-300 years after the onset show in fig. 13 (and fig. 14). The temporal changes in temperature profiles in the SO (see fig. 15) show that contour lines of heat approach the Antarctic as the strong barrier of ACC is disturbed. The ACC which was otherwise blocking the heat from penetrating it does now lets the heat migrate toward the South. This explains why we saw both temperature increases in Greenland and a more gradual and sparse warming of Antarctica (fig. 9). The isopycnals outcrop around 50 °S in the SO during the interstadial mode (see fig. 15).

The temperature signal is initially strongest at 1000 m depth after the interstadial onset (as shown in fig. 13). From CESM data output we get a time-lag in the initial response of approx. 150±5 years between the two latitudes, the warming starts later the more southerly we look but we get an

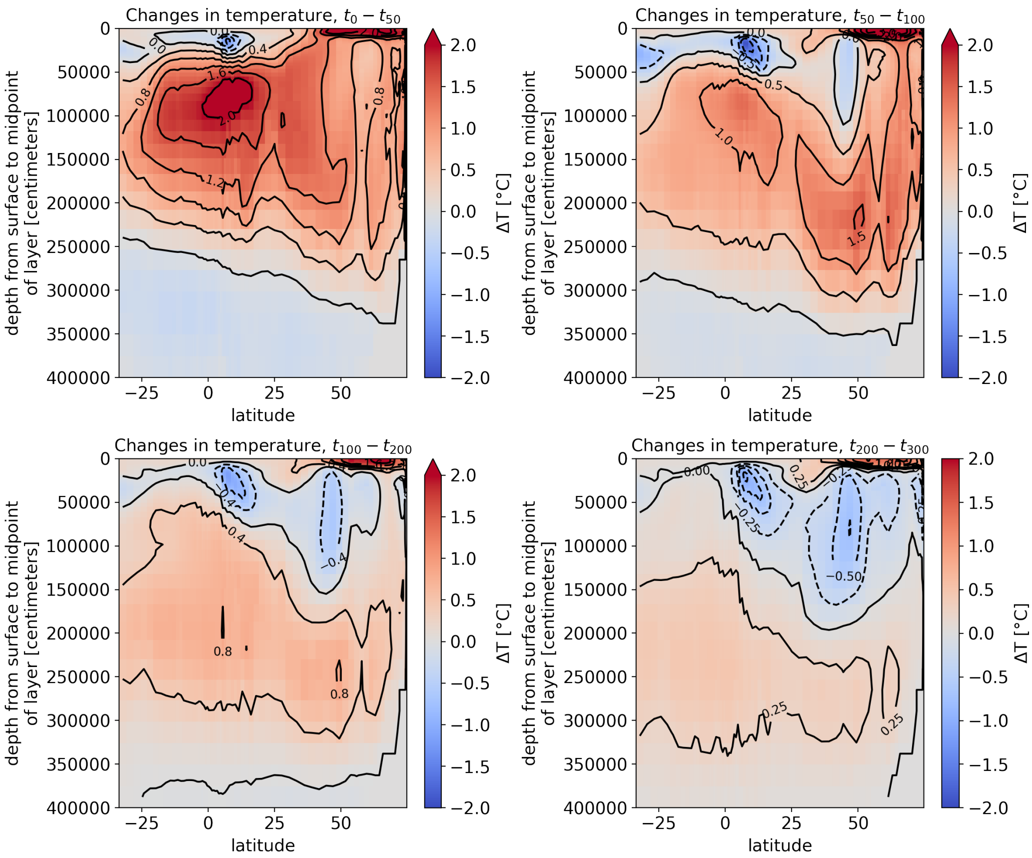

Figure 14: After interstadial: temporal temperature anomaly adjustments in the Atlantic.

instantaneous cooling before this. Besides it the far most southern signal becomes triangular or linear compared to outputs from Veros (see the attached paper in A.1). If the hypothesis hold, then this is due to the difference in domain structure and size. In Veros, the domain is an ocean-only model which is isolated from other basins and this gives a small distance in which the boundary waves can travel and diffuse through to reach a given latitude. Small distances and complete isolation give a relatively fast signal propagation toward the south. However, CESM1 is a fully coupled global climate model i.e. it contains other basins as well as atmospheric and sea-ice models. The interpretation is that as the signal has to diffuse through greater and greater distances the response becomes more linear and the D-O switch between warm and cold periods in the North becomes more triangular in waveform (in the Southern Ocean) as it is seen in the Antarctic ice cores. This would become especially significant as the temperature is diffused around Antarctica in latitude and depth. A way to test this hypothesis is to look at various latitudes in the Pacific. Along with the boundaries that encircle the Indian and

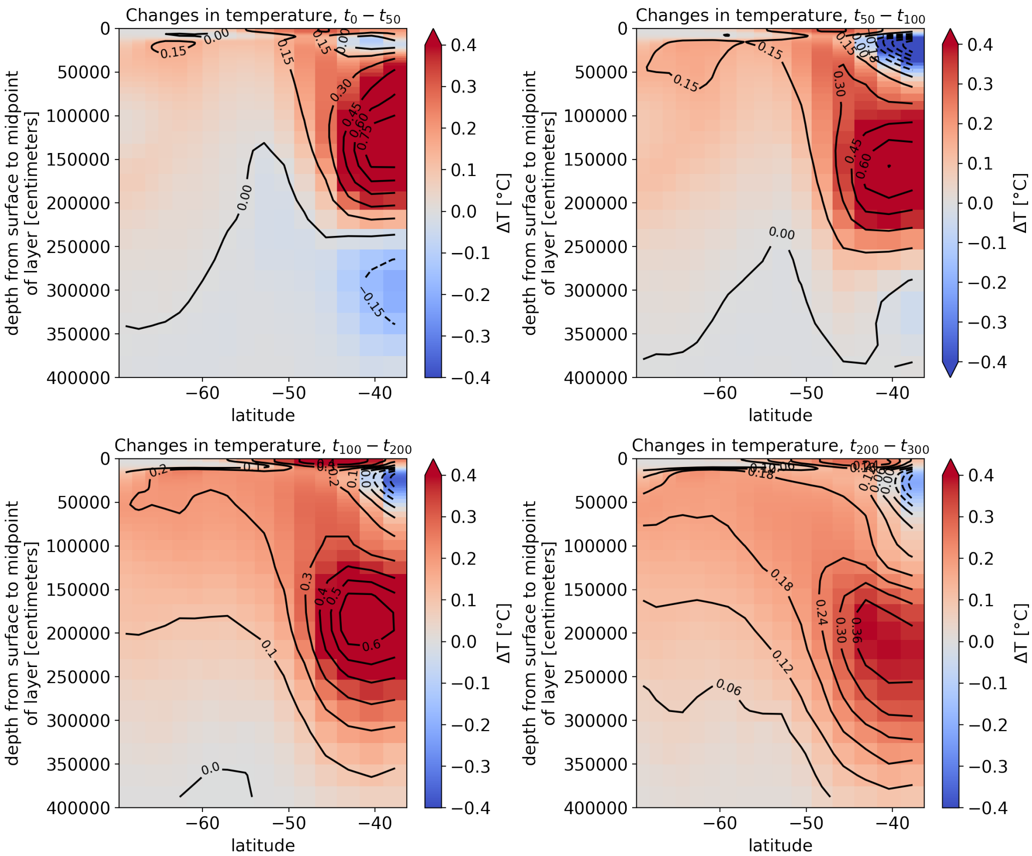

Figure 15: After interstadial: temporal temperature anomaly adjustments in the Atlantic section of the Southern Ocean.

Pacific Oceans and the ACC which connects all the ocean basins, we think that sea-ice in the high polar regions may also have an impact on the delay in the warming of the Southern Ocean. One could imagine that sea-ice slows down the process which is responsible for transferring heat to the polar regions. In an attempt to verify or reject this interpretation we looked at profiles for changes in sea-ice at 50°S and 60°S, respectively. The model shows that there are intermediate time-lags in the signal propagation through the Atlantic into the SO (see figure 16). The timings which are marked with dashed lines are listed in table 1.

The relative temperature profiles at 300 m depth in the S. Atl. and the SO, in fig. 16, visualize the many factors that affect the subsurface sea temperatures due to climatic transitions, and the intermediate time-lags are a consequence of the tightly coupled complex system of the Earth. The signal in the 300 m depth is comparable to the 500 m depth in the result for the Atlantic Ocean

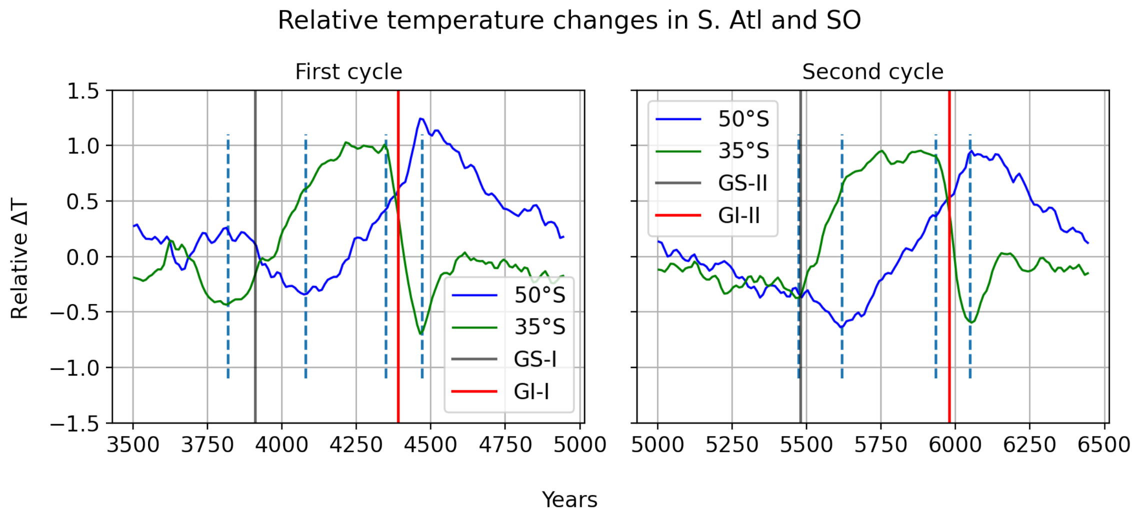

Figure 16: Relative temperature changes at 300 m depth in S. Atlantic (35°S) and Southern Ocean (50°S). The gray and red vertical lines represent the Greenland stadial (GS) and Greenland interstadial (GI) which is defined according to Greenland surface air temperature. The grey dashed lines mark: the response time in 35°S; the response time in 50°S; the adjustment time in 35°S; the adjustment time in 50°S.

presented in Pedro et. al. [15]. The North and South Atlantic temperature contrasts are confined to the upper 500 m during the interstadial, in model outputs from CESM, this is different from the results from Pedro et. al. [15] where the contrasts are expanded down to 1 km below the sea surface. Same applies for the stadial, the N. Atlantic cooling signal reaches greater depths in Community Climate System Model version 3 (CCSM3) compared to outputs from CESM1. The 300 m depth relative temperature profile reveal the time-lag and the process being responsible for propagating the ocean signal from the S. Atl into the SO across the ACC. The signal propagation through the Atlantic ocean happens on a slow timescale of several hundred years (see table 1), the response time is the initiation time where the basin starts to react while the adjustment time it finishes adjusting to the new climate, the difference between these two quantities reveal the time it took the basin to adjust. The vertical lines in fig 16 denoting the stadials and interstadials reveal that just as the South Atlantic is getting warmer the Southern Ocean gets colder (along with the North Atlantic which is not shown here explicitly). This happens during both of the (Greenland) stadials generated from the model, and it lasts approx

site/"cycle"	r	a	$a-r$
35°S / I	3820	4350	530
50°S / I	4080	4470	390
35°S / II	5474	5935	461
50°S / II	5620	6050	430

Table 1: A table of the times (in model year) marked as dashed vertical lines in fig. 16. The abbreviations are response (r) and adjustment (a) time and the difference between them. The resulting time-lags between the ocean adjustment in 35°S and 50°S is: 120±10 years (during the first stadial/interstadial cycle); and 115±10 years (during the second cycle). Based on both cycles, the average time-lag between the responses is 203±10 years.

200 years until a warming trend takes over (while the S. Atlantic has adjusted more than 60%). Once the South Atlantic has fully adjusted it releases heat to the North Atlantic via the strengthened AMOC and southward with eddy advective transports (chapter 6 explains further how heat crosses the ACC). However, the adjustment of the Southern Ocean is completed simultaneously with complete depletion of heat in the South Atlantic. The average time between the adjustment of Southern Ocean and South Atlantic is 118 ± 10 years and 203±10 years for the responses. The time-lags between the DO-cycles and AIM were 140 ± 10 years and 150 ± 10 years according to the modelled surface air temperatures at NGRIP and EDML sites respectively (see Appendix A.2). The measured time-lags in the oceans gives some indication of a delayed dynamics which matches the observed bipolar seesaw time-lag of 208 ± 96 years[15]. In the figures of the in-depth profiles of temperature changes in the interstadial Atlantic Ocean, it was shown that the maximum temperature increase occurs at the 1000 m depth. In the following figures, fig. 18 and the Hovmöller diagram in fig. 20, the intriguing question is *when and how does the heat enter* $50-55°S$*?* A suggestion for the possible mechanism behind it is given in the following text. The the barotropic stream-function is suggested to be involved.

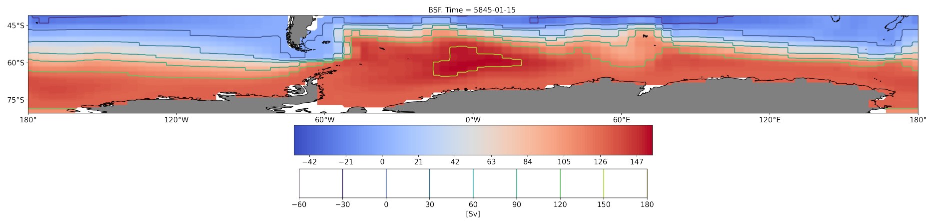

Figure 17: A map of the barotropic stream-function is presented for the Southern Ocean. The ACC is the fast flowing current in eastward (positive) direction which appears in red contours, while the blue contours are flowing in westward direction. The strong Weddell gyre is visible with its contours near 0°W. There is a lot of structure in the zonal flow with can operate as pathways for oceanic signals moving across the ACC. The strength is from -42 to 147 sverdrup.

The Hovmöller diagram in fig. 20 visualizes that the southward migration of heat and diffusion are not the only mechanisms which are responsible for warming the Southern Ocean and Antarctica. A closer look at the second cycle shows that the time where the heat is being trapped in the far South by an extra pathway is occurring around year 6000 in the model. A temperature anomaly map of Antarctica around this period is considered in more detail in fig. 19. The ACC contains a lot of zonal structure which is making up alternative paths for letting heat enter Antarctica, it has a tilt toward the South between 102°W and 60°W where the water flows with the Drake Passage, and it contains two large gyres, the Ross and Weddell gyre. The Weddell Gyre is a more strong rotating ocean gyre compared to Ross gyre (see fig. 17). The southward tilt of ACC near the drake passage and the Weddell gyre can both be argued as being pathways for letting heat enter the South Pole. It appears in the close look at the region of ACC that there are large changes in heat contours in the location of the Weddell around 0°W. A circular heat path is evolving with time around 0°W in the location of the Weddell Gyre, and this pathway circulates heat clockwise into the Antarctica continent. The circular appearance initiated from the Weddell gyre is most clear in the subplot for model year 6045-6095 in fig. 19. The other pathway in the regions west to the Drake passage is also important as

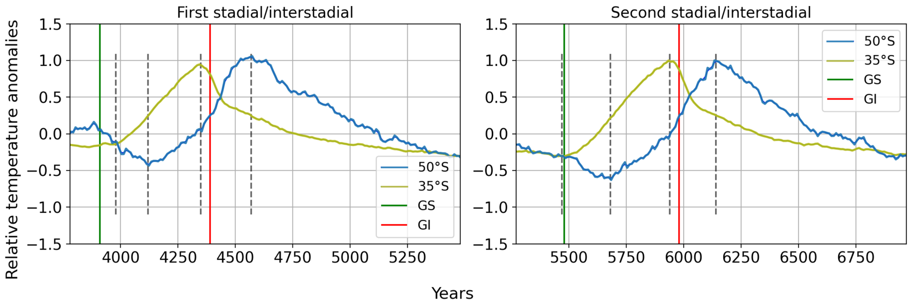

Figure 18: Relative temperature changes at 1000m depth in the Atlantic Ocean based on CESM1 outputs. The green and red vertical lines represents the Greenland stadial (GS) and Greenland interstadial (GI) which is defined according to Greenland surface air temperature. The grey dashed lines mark the: the response time in 35°S; the response time at 50°S; the adjustment time at 35°S; the adjustment time in 50°S.

heat can enter in ocean regions west to 60°W via the southward tilt of ACC. Once the heat has come southward enough it is captured by the counter current along the continental boundary where it is flowing westward and merges into the Ross gyre. The Ross gyre is then redistributing the heat over a large portion of the SO and thereby heat up the remaining water.

The model result shows that heat is transferred southward from the North Atlantic with the kelvin waves along the western boundaries and the signal is transported east-ward at the equator and other wave features such as the Rossby waves transport.

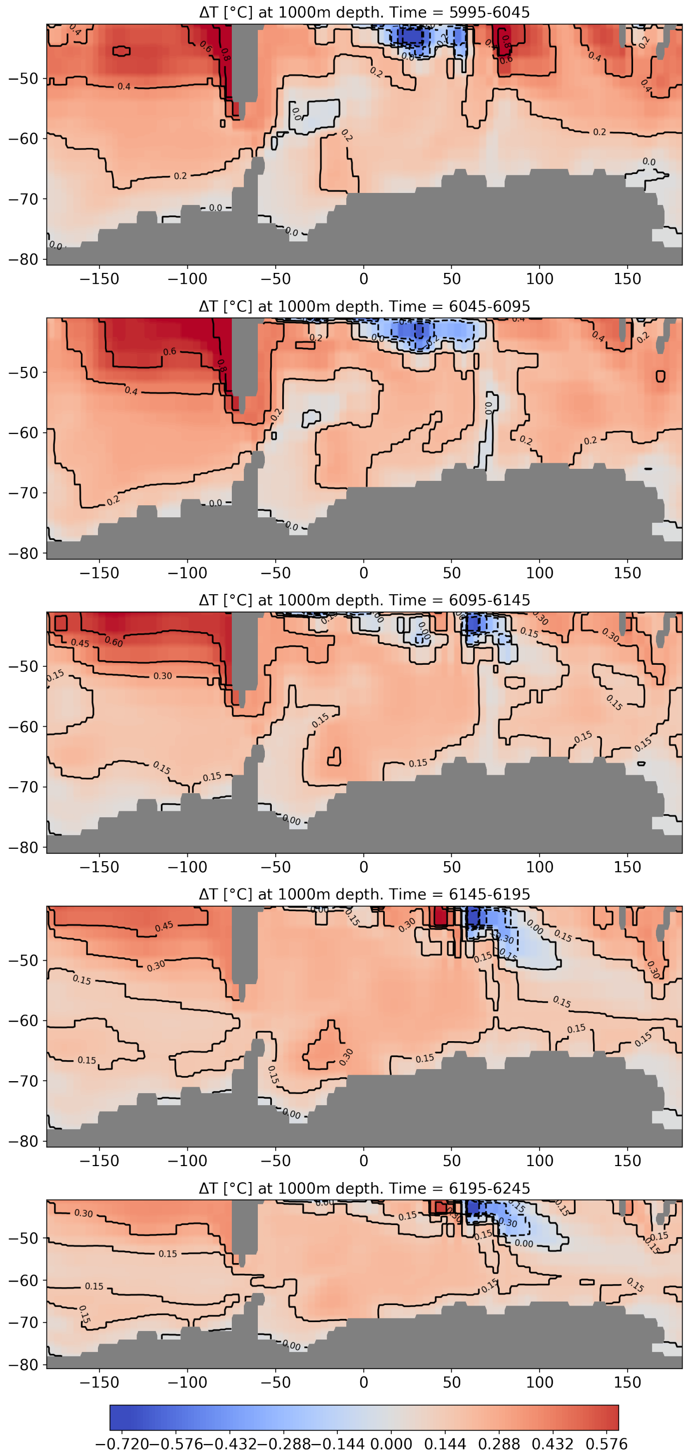

Figure 19: A temperature anomaly map of the Southern Ocean in longitude (east degrees as positive and west degrees negative) and latitude coordinates (north as positive and south as negative). The temperature anomalies are determined for fixed depth at 1000 m below the surface and its numbered contour lines are plotted along with it. Each subplot is presenting the average temperature anomaly between the prescribed time range of 50 years. which shows the temporal changes in the ”heat paths”.

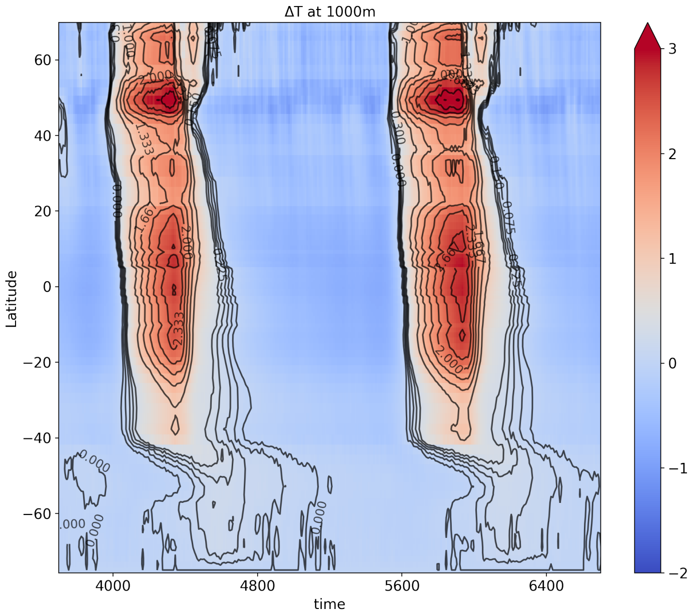

Figure 20: Hovmöller diagram of 1000m depth temperature (in degree Celcius) changes in the Atlantic Ocean. The largest temperature increase during the interstadial was observed within the South Atlantic ocean was observed at this depth.

6

ENERGY COMPARTMENTS DURING THE STADIAL/INTERSTADIAL

The time average of the global zonally averaged ocean heat transport from the coupled model simulation of the D-O oscillation is presented in fig. 21. The model generates self-sufficient DO-cycles, therefore, both are represented in the reconstruction of an mean state for the ocean heat transport processes. The model allows for tracing the different energy components: the total northward heat transport; eulerian-mean advection; eddy-induced advection (bolus) + diffusion; eddy-induced (bolus) advection; submeso advection (see fig. 21). The different energy components makes it possible to eliminate which processes are the most dominant in terms of transferring heat across ACC and thereby heat the Antarctica. In the following Fig. 22, a closer look at the two modes (interstadial and stadial) reveals how and with which process a given latitude receives its heat. The right and the left panels of Fig. 22 shows the deviations from the global averages presented in Fig. 21. During the interstadial the northward transport of ocean heat is stronger in the northern hemisphere relative to the stadial. During the stadial, no heat enters latitudes south of 50 °S via the oceans (see right panel of fig. 22). However, there is on average a net southward heat transport across 50 °S, hereof the eddies and diffusive processes being the most responsible for this transport but the eulerian-mean advection becomes equally important as the eddy-diffusion transport when the latitude band at 56 °S is approached. The contribution to the reduced ocean heat transport during the stadial is mainly from the reduction in the Atlantic Ocean heat transport during the reduced AMOC circulation of the stadial [23]. Our model results displayed in table 2 did in general show a high amplitude of the total

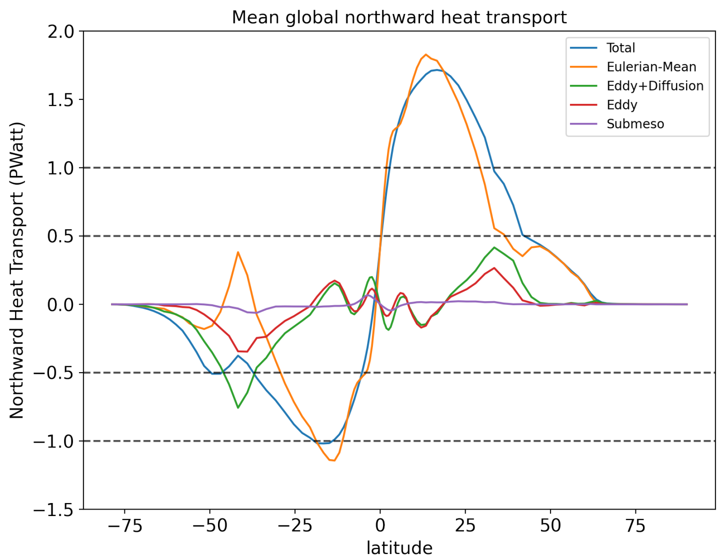

Figure 21: Average global northward heat transport components in CESM1 experiment of LGM. The global average is made over two interstadial-stadial cycles. The Eulerian-mean and the eddy advection/diffusion has opposite signs in the southern Atlantic and in the Southern Ocean, this is one of the reasons we think that eddies are responsible or the dominant term for transferring heat southward.

southward ocean heat transport hereof the eddies and diffusive processes being responsible for up to 67% of this transport during the interstadial. While on average for the whole time series of 300 years (after the interstadial onset), the eddies and diffusion account for approx 60% of the total ocean transport. Both in the case of the stadial onset and the interstadial onset, the northward heat transport components, MOTH_{total} and MOTH_{eddy}, are of higher amplitudes within the first 100 years, hereafter, the signal starts to decrease. These ocean heat fluxes of the interstadial modes are in agreement with the temperature anomalies of the SO shown in fig. 15 where the heat signals were slightly damped after 200-300 years. The results obtained from outputs from CESM are in general different from Pedro et al. (2018) [15]. Unlike the results from Pedro et al. (2018), the Antarctic surface air temperature starts to increase 210 years after the onset of the Greenland stadial (as shown in fig. 23) which is about the same time as when the BSF (the ACC flow) through the Drake Passage has approached its maximum adjustment before it begins to decrease again. Both the zonal flow of ACC through the Drake Passage and the southward traveling eddy fluxes across the ACC increases immediately with

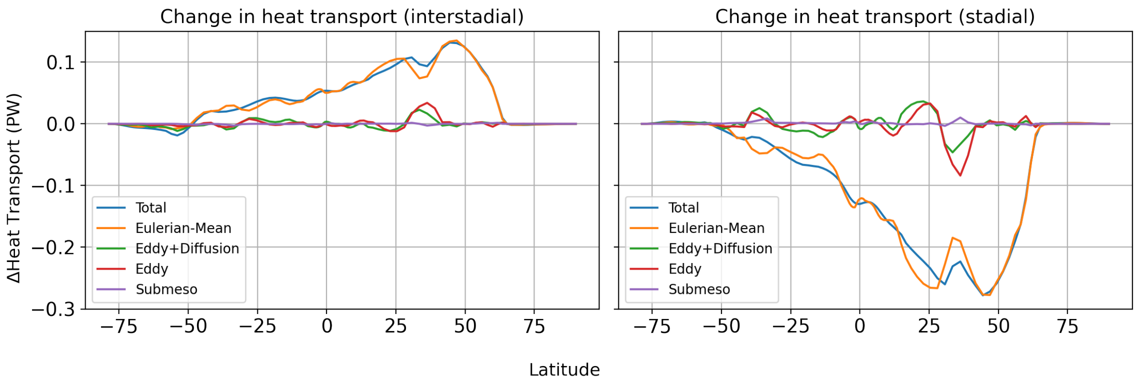

Figure 22: Left figure is the difference between the interstadial and the mean state. Similarly, the right figure is the difference between the stadial and the mean state. These two stages are related to variations in AMOC; the interstadial is defined as the average between $200-300$ years after the AMOC resumption; the stadial is defined as the average between $200-300$ years after the AMOC collapse. AMOC strengths are almost in phase with Greenland surface air temperatures. The global total northward heat transport increases during the warm period and vice versa during the cold period. (For comparison look at figure 4 in Pedro et al (2018) [15])

the initiation of the transition toward the glacial environments. There is a time-lag of 120 years in the mean annual sea ice retreat in the SO $50-70°$S and in the upper ocean temperature increases in the SO $40-55°$S (North of the ACC) and $55-70°$S (South of the ACC). The sea temperatures in the SO $40-55°$S increases exponentially and are more rapid compared to the SO temperature profile further South (across the ACC barrier) where it increases slowly and linearly (see fig. 23). The latitudinal difference has also been noticed in Pedro et al. (2018), it occurs because of two different operating dynamics in the coupled climate model. The first operating mechanism is more sensible and latent heat is released from the ocean in regions of sea ice loss. The other process is more heat being absorbed by the ocean around the polar front. This is a part of the explanation of why the two curves of sea temperature changes on either side of the ACC have different shapes. The results presented in fig. 23 reveals a different sequence of the leads and lags in the Greenland stadial. The higher resolution of the SO in CESM is taking into account more of the dynamic processes in the SO: the southward traveling heat in the eddy fluxes cannot alone heat up the Antarctic or to the extent, it is prescribed

MOHT 55°S			
	0-100 yrs	100-200 yrs	200-300 yrs
(Interstadial)			
MOTH$_{total}$	-39.9 (-1.7)	-33.3 (-15.3)	-18.8 (-18.4)
MOTH$_{eddy}$	-24.5 (-9.1)	-21.8 (-29.4)	-11.6 (-40.7)
(Stadial)			
MOTH$_{total}$	28.1 (1.9)	16.4 (19.6)	3.7 (40.5)
MOTH$_{eddy}$	16.2 (7.4)	15.2 (36.6)	2.9 (48.7)

Table 2: All values are anomalies i.e. deviations from the time-average and the units are in terawatt (TW). CESM1 outputs of the meridional ocean heat transport (MOHT) across ACC at 55°S. The MOHT values in the parentheses are based on outputs from another GCM i.e. Community Climate System Model version 3 (CCSM3) from the comparative study made by Pedro et. al. (2018) [15]. MOTH$_{total}$ is the sum of the Eulerian mean advection and the eddy-induced advection (bolus) + diffusion and the submeso advection, while MOTH$_{eddy}$ is the term entailing the eddy-induced advection and diffusion only. The time-intervals ($0-100$ yr, $100-200$ yrs and $200-300$ yrs) indicates the time range included in the averages, the years are presented as the number of years after the respective termination (of interstadial/stadial).

in the paper by Pedro et al. (2018) [15]. The MOHT$_{eddy}$ is roughly increased by 30 TW from the initiation of the GS to approx 500 years later when the glacial is fully accomplished in the NH, this is 20 TW less than Pedro's study [15] while the Antarctic surface temperature increases are of the same magnitude in both studies. Taking into consideration the zonal structure of the temperature anomalies around the Antarctic and the timescale of the temporal temperature changes, the remainder of the description on how heat enters the south is very likely to be due to the heat pathways in the ACC i.e. the Ross gyre and the southward tilt in the eastward direction on the west-side of Drake Passage (see chapter 5 and fig. 19).

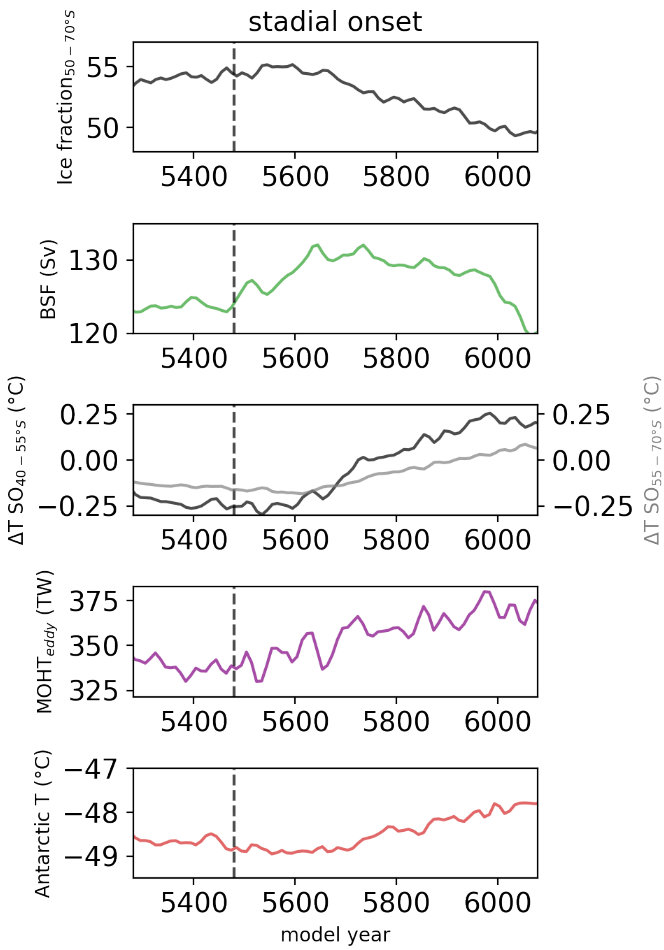

Figure 23: The Greenland stadial onset is marked as a vertical dashed line in all of the four subplots. From the top: sea ice concentration between $50-70°$S; barotropic stream function (BSF) through the Drake Passage; the upper 500 m sea temperature changes in the SO between $40-55°$S (black) and $55-70°$S (gray); the meridional ocean heat transport via eddy fluxes (MOHT$_{eddy}$) across ACC; and the mean annual 70-90°S Antarctic surface temperature.

Part IV

CONCLUSION

7

CONCLUSION

Data outputs from the LGM experiment made in the coupled global climate model CESM1 makes up the base of this study. Thus, understanding the DO cycles and the interhemispheric coupling is a matter of combining observational data samples with well-resolved and descriptive numerical models which capture all of the important dynamics and spatial structure. CESM1 succeeds in this matter with its high details and coupling between the ocean, atmosphere, sea-ice, bio-geochemistry, and its well-resolved SO. A simple method was used as this study dealt with model outputs, the method was to search for exact timings of the interstadial/stadial onsets and compare the determined timings with the variabilities of the individual variable. The first task of this study was to find and verify the different leads and lags to the DO-cycles. The second task was to determine how the heat which was originated in the high northern latitudes travels southward in the SO across the ACC. In the first part, stochastic atmospheric forcing parameters i.e. temporal changes in NAO, wind strengths along with their relative timing have been compared to the sea-ice fraction changes in the southern regions in the Icelandic ocean. The ocean regions in the south of Iceland were the region that appeared as the most sensitive and variable due to climatic transitions, it was therefore used as the indicator or proxy for the general sea ice patterns of the NH. The long-term variations in NAO and wind stress reveals that the atmosphere is of minor dominance, and pressure and wind changes in the NH are not sufficient enough to break the sea-ice in the polar seas (as it was shown in fig. 4 and fig. 3). However, winds tend to adjust their strength according to the presence of sea-ice (see fig. 4). The northward travelling heat signal in the upper SO (in fig. 3), temperature and salinity changes in the seawater columns have appeared as an important driver in terms of leading the DO cycles (shown in fig. 7 and fig. 8). During the cold stadial conditions heat was being trapped in the depths of NA (see fig. 10, fig. 11) which brought the system into an unstable environment with warmer waters underneath the colder water. Diffusive processes are believed to initiate the expansions of heat in the water columns of the Nordic Sea, and Labrador and Irminger Seas which causes the sea ice to break and force the climate system into interstadial conditions (as described in fig. 7 and fig. 8).

In the other task, the interhemispheric time-lag was studied. We have found various delay in the signal propagation - depending on which reservoir we looked at. The average time-lag between the oceanic responses is 203$\pm$10 years and 118 $\pm$10 years between the fully adjustment after the signal has been transmitted 1. The average modelled atmospheric time-lag between the DO onset at the NGRIP site and the AIM at the EDML site is 145 $\pm$10 years, while the determination over the entire Antarctic and Greenland (in the model domain) reveals a time-lag 210$\pm$10 years (according to the results in figure 3, and as described in chap. 6 and shown in appendix A.2). The time-lag between DO events and AIM reveal the time it takes the heat to travel from the high northern latitudes across the ACC. Advection and wave propagation could not cross the ACC in the depths where temperature signal was strongest i.e. in the upper 1000 m, therefore, eddy fluxes and and diffusion are among the processes that are responsible for moving the signal from the SA to the SO. However, the analysis of energy components did not match the results obtained by Pedro et. al (2018) [15], eddy fluxes dominate ocean heat budget in the SO but it does not exceed the eulerian mean flow (see Table 2). The Antarctic temperature changes were of the same magnitude as presented in [15] but the variability of the southward MOHT across ACC was sparse. In an attempt to find a vast explanation, other processes which have not been investigated before were looked upon, as one shall take full advantage of the high resolution of the SO which CESM1 provides for. The ACC is the worlds fastest moving current, its zonal structure generates two large gyres which has shown to play an important role in capturing the southward travelling heat. The results for the temperature changes in the SO which were presented in fig. 19 and fig. 25 showed that a southward (horizontal) tilt of the BSF in the west to east direction toward the Drake passage made up a hot-spot and it acts as a pathway for the heat, the other heat pathway discovered is the Weddel gyre near 0°W which is also responsible circulating the heat into the SO and redistribute it and thereby warm-up Antarctica.

REFERENCES

[1] Niklas Boers, Michael Ghil, and Denis-Didier Rousseau. "Ocean circulation, ice shelf, and sea ice interactions explain Dansgaard–Oeschger cycles". In: *Proceedings of the National Academy of Sciences* 115.47 (2018), E11005–E11014. ISSN: 0027-8424. DOI: 10.1073/pnas.1802573115. eprint: https://www.pnas.org/content/115/47/E11005.full.pdf. URL: https://www.pnas.org/content/115/47/E11005.

[2] W. S. Broecker, D. M. Peteet, and D. Rind. "Does the ocean-atmosphere system have more than one stable mode of operation?" In: *Nature* 315 (1985), pp. 21–26. DOI: 10.1038/315021a0.

[3] Wallace S. Broecker, Dorothy M. Peteet, and David Rind. "Does the ocean–atmosphere system have more than one stable mode of operation?" In: *Nature* 315.21–26 (May 1985). DOI: 10.1038/315021a0. URL: https://doi.org/10.1038/315021a0.

[4] K. Bryan and L. J. Lewis. "A water mass model of the World Ocean". In: *Journal of Geophysical Research: Oceans* 84.C5 (1979), pp. 2503–2517. DOI: https://doi.org/10.1029/JC084iC05p02503. eprint: https://agupubs.onlinelibrary.wiley.com/doi/pdf/10.1029/JC084iC05p02503. URL: https://agupubs.onlinelibrary.wiley.com/doi/abs/10.1029/JC084iC05p02503.

[5] Gokhan Danabasoglu and John Marshall. "Effects of vertical variations of thickness diffusivity in an ocean general circulation model". In: *Ocean Modelling* 18.2 (2007), pp. 122–141. ISSN: 1463-5003. DOI: https://doi.org/10.1016/j.ocemod.2007.03.006. URL: http://www.sciencedirect.com/science/article/pii/S1463500307000431.

[6] K. A. Donohue et al. “Mean Antarctic Circumpolar Current transport measured in Drake Passage”. In: *Geophysical Research Letters* 43.22 (2016), pp. 11, 760–11, 767. DOI: https://doi.org/10.1002/2016GL070319. eprint: https://agupubs.onlinelibrary.wiley.com/doi/pdf/10.1002/2016GL070319. URL: https://agupubs.onlinelibrary.wiley.com/doi/abs/10.1002/2016GL070319.

[7] Peter R. Gent and James C. Mcwilliams. “Isopycnal Mixing in Ocean Circulation Models”. In: *Journal of Physical Oceanography* 20.1 (1Jan. 1990), pp. 150–155. DOI: 10.1175/1520-0485(1990)020<0150:IMIOCM>2.0.CO;2. URL: https://journals.ametsoc.org/view/journals/phoc/20/1/1520-0485_1990_020_0150_imiocm_2_0_co_2.xml.

[8] H. Goosse. *Introduction to climate dynamics and climate modeling / Hugues Goosse.* eng. Universite Catholique de Louvain, 2010.

[9] D. Häfner et al. “Veros v0.1 – a fast and versatile ocean simulator in pure Python”. In: *Geoscientific Model Development* 11.8 (2018), pp. 3299–3312. DOI: 10.5194/gmd-11-3299-2018. URL: https://gmd.copernicus.org/articles/11/3299/2018/.

[10] Hannah Kleppin et al. “Stochastic Atmospheric Forcing as a Cause of Greenland Climate Transitions”. In: *Journal of Climate* 28.19 (Sept. 2015), pp. 7741–7763. ISSN: 0894-8755. DOI: 10.1175/JCLI-D-14-00728.1. eprint: https://journals.ametsoc.org/jcli/article-pdf/28/19/7741/4054242/jcli-d-14-00728_1.pdf. URL: https://doi.org/10.1175/JCLI-D-14-00728.1.

[11] Camille Li and Andreas Born. “Coupled atmosphere-ice-ocean dynamics in Dansgaard-Oeschger events”. In: *Quaternary Science Reviews* 203 (2019), pp. 1–20. ISSN: 0277-3791. DOI: https://doi.org/10.1016/j.quascirev.2018.10.031. URL: http://www.sciencedirect.com/science/article/pii/S0277379118305705.

[12] "Chapter 5 The T-S Diagram and Its Properties". In: *Temperature - Salinity Analysis of World Ocean Waters*. Ed. by O.I. Mamayev. Vol. 11. Elsevier Oceanography Series. Elsevier, 1975, pp. 119–158. DOI: https://doi.org/10.1016/S0422-9894(08)71172-3. URL: https://www.sciencedirect.com/science/article/pii/S0422989408711723.

[13] Karl J. F. Meier et al. "Role of the Tropical Atlantic for the Interhemispheric Heat Transport During the Last Deglaciation". In: *Paleoceanography and Paleoclimatology* 36.5 (2021). e2020PA004107 2020PA004107, e2020PA004107. DOI: https://doi.org/10.1029/2020PA004107. eprint: https://agupubs.onlinelibrary.wiley.com/doi/pdf/10.1029/2020PA004107. URL: https://agupubs.onlinelibrary.wiley.com/doi/abs/10.1029/2020PA004107.

[14] WAIS Divide Project Members. "Precise interpolar phasing of abrupt climate change during the last ice age." In: *Nature* 520.7549 (2015), pp. 661–665. DOI: 10.1038/nature14401. URL: https://doi.org/10.1038/nature14401.

[15] Joel B. Pedro et al. "Beyond the bipolar seesaw: Toward a process understanding of interhemispheric coupling". In: *Quaternary Science Reviews* 192 (2018), pp. 27–46. ISSN: 0277-3791. DOI: https://doi.org/10.1016/j.quascirev.2018.05.005. URL: http://www.sciencedirect.com/science/article/pii/S0277379117310351.

[16] W. R. Peltier, D. F. Argus, and R. Drummond. "Space geodesy constrains ice age terminal deglaciation: The global ICE-6G_C (VM5a) model". In: *Journal of Geophysical Research: Solid Earth* 120.1 (2015), pp. 450–487. DOI: https://doi.org/10.1002/2014JB011176. eprint: https://agupubs.onlinelibrary.wiley.com/doi/pdf/10.1002/2014JB011176. URL: https://agupubs.onlinelibrary.wiley.com/doi/abs/10.1002/2014JB011176.

[17] Sune O. Rasmussen et al. “A stratigraphic framework for abrupt climatic changes during the Last Glacial period based on three synchronized Greenland ice-core records: refining and extending the INTIMATE event stratigraphy”. In: *Quaternary Science Reviews* 106 (2014). Dating, Synthesis, and Interpretation of Palaeoclimatic Records and Model-data Integration: Advances of the INTIMATE project(INTegration of Ice core, Marine and TErrestrial records, COST Action ES0907), pp. 14–28. ISSN: 0277-3791. DOI: https://doi.org/10.1016/j.quascirev.2014.09.007. URL: https://www.sciencedirect.com/science/article/pii/S0277379114003485.

[18] W. F. (William F.) Ruddiman. *Earth's climate : past and future / William F. Ruddiman*. eng. 3rd ed. New York: W.H. Freeman, 2014. ISBN: 9781429255257.

[19] Marit-Solveig Seidenkrantz et al. “Evidence for influx of Atlantic water masses to the Labrador Sea during the Last Glacial Maximum”. In: *Scientific Reports* 11.1 (Mar. 2021), p. 6788. ISSN: 2045-2322. DOI: 10.1038/s41598-021-86224-z. URL: https://doi.org/10.1038/s41598-021-86224-z.

[20] Thomas F. Stocker and Sigfùs J. Johnsen. “A minimum thermodynamic model for the bipolar seesaw”. In: *Paleoceanography* 18.4 (2003). DOI: https://doi.org/10.1029/2003PA000920. eprint: https://agupubs.onlinelibrary.wiley.com/doi/pdf/10.1029/2003PA000920. URL: https://agupubs.onlinelibrary.wiley.com/doi/abs/10.1029/2003PA000920.

[21] HENRY STOMMEL. “Thermohaline Convection with Two Stable Regimes of Flow”. In: *Tellus* 13.2 (1961), pp. 224–230. DOI: 10.1111/j.2153-3490.1961.tb00079.x. eprint: https://onlinelibrary.wiley.com/doi/pdf/10.1111/j.2153-3490.1961.tb00079.x. URL: https://onlinelibrary.wiley.com/doi/abs/10.1111/j.2153-3490.1961.tb00079.x.

[22] Guido Vettoretti and W. Richard Peltier. "Fast Physics and Slow Physics in the Nonlinear Dansgaard–Oeschger Relaxation Oscillation". In: *Journal of Climate* 31.9 (Mar. 2018), pp. 3423–3449. ISSN: 0894-8755. DOI: 10.1175/JCLI-D-17-0559.1. eprint: https://journals.ametsoc.org/jcli/article-pdf/31/9/3423/4709371/jcli-d-17-0559_1.pdf. URL: https://doi.org/10.1175/JCLI-D-17-0559.1.

[23] Guido Vettoretti and W. Richard Peltier. "Interhemispheric air temperature phase relationships in the nonlinear Dansgaard-Oeschger oscillation". In: *Geophysical Research Letters* 42.4 (2015), pp. 1180–1189. DOI: https://doi.org/10.1002/2014GL062898. eprint: https://agupubs.onlinelibrary.wiley.com/doi/pdf/10.1002/2014GL062898. URL: https://agupubs.onlinelibrary.wiley.com/doi/abs/10.1002/2014GL062898.

A

APPENDIX

A.1 UNPUBLISHED PAPER: THE GREENLAND CLIPPER: A FAST OCEAN CONNECTION BETWEEN GREENLAND AND ANTARCTICA

The paper[1] continues on the next page.

1 Submitted to Ocean Modelling on April 2021 by Laurits S. Andreasen, Markus Jochum, Guido Vettoretti, Roman Nuterman, Anna S. von der Heydt.

The Greenland Clipper: a fast ocean connection between Greenland and Antarctica

Laurits S. Andreasen[a,b], Markus Jochum[a], Guido Vettoretti[a], Roman Nuterman[a], Anna S. von der Heydt[b]

[a] *TeamOcean, Niels Bohr Institute, Copenhagen, Denmark*
[b] *Institute for Marine and Atmospheric research Utrecht (IMAU), Department of Physics, Utrecht University, Netherlands*

Abstract

An ocean general circulation model is used to investigate the mechanisms that control the time it takes for a North Atlantic perturbation to reach the Southern Ocean and cross the Antarctic Circumpolar Current. This is motivated by the observed anti-correlation between Greenland and Antarctic temperature during the last ice age, which is often referred to as the bipolar see-saw. It is found that the first signs of a North Atlantic density perturbation can be seen in the Southern Ocean after less than 10 years, whereas the transmission of the majority of the signal can take approximately 100 years. Sensitivity studies reveal that the latter timescale is controlled not only by (parameterized) eddy fluxes in the Southern Ocean, but also by the basin width of the South Atlantic. Surprisingly it is found that in the limit of large but not unrealistic eddy fluxes the time scale is determined by the basin width only.

Keywords: Bipolar Seesaw, Atlantic Overturning Circulation, eddy heat transport

1. Introduction

The climates of the two hemispheres of Earth are connected, most prominently seen in the comparison of Greenland and Antarctic temperatures

Email address: `l.s.andreasen@uu.nl` ()

Preprint submitted to Ocean modelling *April 7, 2021*

(Stocker and Johnsen (2003)). During the last ice age sudden rises in Greenland temperature, so called Dansgaard-Oescher (DO) warming events, are followed by a delayed and more gradual fall in Antarctic temperature, the so called Antarctic Isoptope Maxima (AIM). In the same way sudden drops in Greenland temperatures at the end of warm interstadials are followed by a delayed increase in Antarctic temperatures. This overall covariation is known as the bipolar seesaw. The delay between the northern and the southern polar signals, which we will term the Bipolar Seesaw Time Lag (BSTL), has been estimated from different synchronisation methods between Greenland and Antarctic ice cores yielding a $\sim$200 year time lag using ice-core methane synchronization (e.g. WAIS Divide Project Members (2015), Buizert et al. (2018)) and, more recently, $\sim$100 years using bipolar synchronized volcanic eruptions (Svensson, 2020). This time scale applies for both the initiation and terminations of interstadials. Throughout this paper we will assume that the BSTL is of order of $\sim$100 years.

While DO warming events and associated AIMs including their delay have been known from observations since quite some time (Broecker (1998)), it is only more recently that various Earth System Models (ESMs) have been able to reproduce the DO/AIM signal (Peltier and Vettoretti (2014), Pedro et al. (2018), Nielsen et al. (2019)). From both observations and model experiments a consensus is emerging that DO events are initiated by rapid changes to the Atlantic Meridional Overturning Circulation (AMOC) and North Atlantic sea-ice cover (Li and Born, 2019).

What is less well understood is what sets the time scale of the delay between the North Atlantic (NA) and Antarctica. Observations (Barker and Diz (2014)) and models (Vettoretti and Peltier (2015)) suggest that when the NA cools (i.e. during stadials), heat accumulates in the tropical and mid-latitude Atlantic. The heat is then mixed across the ACC by mesoscale eddies resulting in sea-ice melt and sea-ice albedo increases that enhance the warming and ultimately warms Antarctica (Pedro et al. (2018)). Recently it has been proposed that heat transport across the equator could play a role for the BSTL (MorenoChamarro et al. (2020)). Thus, there are numerous processes that could control the BSTL, but Schmittner et al. (2003) have proposed that the slowest timescale is related to mesoscale mixing across the Antarctic Circumpolar Current (ACC). We will focus on testing this hypothesis in the present study.

In a first set of experiments, we globally changed the strength of ocean mesoscale mixing by about 30% in the a low-resolution CESM setup of a version of glacial climate that simulates unforced DO oscillations (Vettoretti and Peltier (2018)). The resulting Greenland and Antarctic temperature anomalies under these altered mesoscale mixing parameters are shown in Figure 1. While the typical time scale of the complete DO/AIM cycle is clearly affected by such mesoscale mixing parameter changes, an effect on the delay (or BSTL) time scale is not obvious. However, for practical reasons the parameter values cannot be changed by more than 30%, and the existence of other modes of variability made it impossible to rule out that the time-lag is indeed independent of the eddy strength as Figure 1 may suggest. In this paper, we therefore address the following question: How long does it take for the Southern Ocean (SO) to start warming after the AMOC collapsed, and which (ocean) processes control the delay? The case of AMOC amplification was also studied, but since it gave the exact same results as the collapse, only the latter is presented here.

In investigating the total delay between Greenland and Antarctic temperature signals, we will not discuss the mechanisms associated with the initial cause of the changes in the high northern latitudes leading to the AMOC collapse. Neither are we concerned with the processes that transport the signal from the SO and onward to Antarctica, once the SO becomes warm enough to melt the sea ice from below. Instead, we focus only on how the northern ocean signal reaches the high southern latitudes. A review of the theoretical literature suggests three different processes that may control the time scale:

1) *Adiabatic adjustments in the Atlantic basin:* As argued by Kawase (1987), a change in the density field can be communicated along the western boundary of the North Atlantic, propagate from west to east along the equator and continue southward in the other hemisphere as an eastern boundary wave in the South Atlantic. These changes are then conveyed to the basin interior by Rossby waves, which are emitted by the boundary waves.

More careful evaluation reveals that the boundary wave, once it has reached the eastern boundary of the South Atlantic, has to continuously adjust to a decreasing Rossby radius of deformation as it travels southward. This adjustment leads to wave scattering, resulting in a geostrophic flow along the eastern boundary[1] (McWilliams (2006)). This current transports

[1]One way to think about this is that the changing properties of the boundaries will give a gradient in the Reynolds stress of the wave. This will induce a mean flow.

water southward, and is the main component of the adjustment process (Marshall and Johnson, 2013). Since the current is in geostrophic balance, it is supported by a sloping density anomaly. At the eastern boundary such an anomaly is vulnerable: It will leak westward into the interior as radiated Rossby waves. Since the Rossby wave propagation speed is fast compared to the overall adjustment, the radiation process will keep the anomaly and hence the geostrophic transport small (Johnson and Marhsall, 2002). In other words, the boundary wave constantly tries to build up a density anomaly transport, whereas the Rossby waves tries to smear out the density anomaly. Some of the Rossby waves may break up into baroclinic eddies, but this does not alter the overall analysis (Lacasce and Pedlosky (2004)).

In a two-layer model we can estimate the time it takes the ocean to adjust to these processes: The eastern boundary anomaly gives a zonal pressure gradient with magnitude $p_x \sim \rho g' H/L_d$, where H is the depth of the upper ocean affected by the perturbation, L_d is the Rossby radius of deformation, g' is the buoyancy of the upper layer and ρ the ocean density. The anomaly is in geostrophic balance and gives a volume flux, $Q \sim v_{\mathrm{g}} H L_x$, where v_{g} is the geostrophic velocity and L_x the width of the basin. We can estimate v_{g} at the southern edge of the basin:

$$v_{\mathrm{g}} f_{\mathrm{s}} \sim \frac{g' H}{L_x}, \tag{1}$$

where f_{s} is the Coriolis parameter at the southern edge of the basin. The upper ocean has volume $V = A\ H$, A being the surface area, and the time it takes Q to impact the upper layer is

$$\tau_{\mathrm{adi}} \sim \frac{V}{Q} \sim \frac{f_{\mathrm{s}} A}{g' H}. \tag{2}$$

Johnson and Marhsall (2002) arrive at the same time scale from a more thorough analysis, and find that τ_{adi} is the e-folding time of the adjustment for the upper ocean to a perturbation in deep water formation. Using $g' = 0.01$ m/s^2, $f_{\mathrm{s}} = 10^{-4}\mathrm{s}^{-1}$, $H = 300$ m and A from Table 1, we get $\tau_{\mathrm{adi}} = 30$ years. Since this is an e-folding time, it is plausible that it can explain the observed 100 year lag of Svensson (2020).

2) *Adiabatic adjustments in the Southern Ocean*: The processes involved so far require meridional boundaries to travel south. Therefore, our considerations so far lead to a signal from the perturbation that is stranded at the

southern border of the Atlantic Ocean. Hence the waves can't cross the ACC and reach Antarctica.

As suggested by Schmittner et al. (2003), baroclinic eddies in the SO must play a key role in the heat transport across the ACC. Effects of baroclinic eddies on the mean flow act to flatten isopycnals and to transport tracers along isopycnals (Gent et al. (1995)). The baroclinic eddies are not resolved in most ocean models used for climate studies, and are instead parameterized by isopycnal (Redi (1982)) diffusion and a parameterized eddy advection ("bolus velocity", Gent and Mcwilliams (1990), Griffies (2003)). The strength of the latter depends on the slope of isopycnals s, and a parameter κ_{GM}, often termed the eddy transfer coefficient. The actual structure of κ_{GM} is still a matter of debate, but it appears that at least for the SO these parametrizations can reproduce much of the eddy effects seen in eddy resolving models (Poulsen et al. (2018), Viebahn et al. (2016)).

The transport velocity of the (parametrized) SO eddies scales as $v_{\mathrm{bolus}} \sim \kappa_{\mathrm{GM}} \cdot s_z$, where s_z is the vertical derivative of the slope, s, of the isopycnals in the SO. The slope scales as $s \sim H/L_{\mathrm{s}}$, where L_{s} is the distance between the southern tip of the South Atlantic and the ACC core. Hence $s_z \sim s/H = 1/L_{\mathrm{s}}$. This gives an eddy advection time scale of

$$\tau_{\mathrm{eddy}} \sim \frac{L_{\mathrm{s}}}{v_{bolus}} \sim \frac{L_{\mathrm{s}}}{\kappa_{\mathrm{GM}} s_z} \sim \frac{L_{\mathrm{s}}^2}{\kappa_{\mathrm{GM}}}, \tag{3}$$

and appears similar to a diffusive time scale, in good agreement with the relation between eddy advection and thickness diffusion. Taking $L_{\mathrm{s}} = 10°$, the distance between southern tip of the basin and the center of the channel in our model, and κ_{GM} of 1000 m^2/s, yields a $\tau_{\mathrm{eddy}} \approx 40$ years. Therefore this timescale is also comparable to the BSTL.

3) *Diabatic adjustments*: Adiabatic adjustments alone cannot change the heat content of a water parcel. To achieve heat content changes, a water parcel needs to be in contact with the surface, or it must pick up heat from nearby parcels via heat diffusion. Samelson (2011) and Allison et al. (2011) give a detailed analysis of the role of diapycnal heat diffusion for this type of adjustments. Here we only mention that the time scale associated with the diffusion equation and hence diapycnal heat diffusion is

$$\tau_{\mathrm{diff}} \sim \frac{\Delta H^2}{K_{\mathrm{v}}}, \tag{4}$$

where ΔH is isothermal deepening. If we take $\Delta H = 100$ m to be the thickness of the thermocline, and $K_\mathrm{v} = 10^{-5} m^2/s$ (Ledwell et al. (1993)) we again arrive at a similar timescale for the BSTL ($\tau_\mathrm{diff} \approx 30$ years).

Therefore, there are five main processes that we expect to have an impact on the adjustment time of the SO, and hence on the BSTL. These processes are: (1) boundary wave propagation, (2) geostrophic transport, (3) Rossby wave propagation, (4) eddy advection and (5) diapycnal diffusion. We have also identified key model parameters involved in setting the time scales of these processes. Figure 2 summarises all processes in their order of occurrence during the signal propagation from the North Atlantic to the Southern Ocean.

The boundary and Rossby wave related processes are, however, very fast such that we do not expect them to have any relevance in determining the BSTL (Marshall and Johnson (2013)). The scaling analysis presented here suggest similar time scales for the remaining three processes ((2), (4) and (5)). From scaling considerations alone we cannot determine the slowest of these processes, which eventually determines the BSTL. Therefore, we have tested these ideas using a full OGCM by addressing the following questions:

1. How does the SO adjustment time depend on adiabatic geostrophic adjustments in the Atlantic basin (Johnson and Marhsall (2002)) - that is on f_s and H as in eq. 2?
2. How does the SO adjustment time depend on baroclinic eddies (Schmittner et al. (2003)) - that is on κ_GM as in eq. 3?
3. How does the SO adjustment time depend on the vertical mixing (Samelson (2011)) - that is on K_v as in eq 4?

The questions are interelated, especially because H depends on κ_GM, K_v and f_s. This can be seen from scaling models of the thickness of the Atlantic thermocline (Gnanadesikan (1999), Nikurashin and Vallis (2011), Vallis (2017)):

$$\frac{g'H^2}{f_\mathrm{n}} + \frac{\kappa_\mathrm{GM} H L_x}{L_\mathrm{s}} \sim \frac{F_\mathrm{SO} L_x}{f_\mathrm{s}} + \frac{K_\mathrm{v} A}{H}. \tag{5}$$

Here f_n is the Coriolis parameter in the NA regions with deep convection and F_SO the SO wind stress. The four terms of eq. 5 correspond to four balancing processes: The upper ocean is drained by deep convection in the northern hemisphere (first term) and by eddies in the SO (second term). At the same time cold water is driven into the upper layer by wind induced

Ekman transport in the SO (third term), and the upper layer grows from diabatic downward heat diffusion (fourth term).

The remainder of this paper is organized as follows. In section 2 we describe the model setup and give details about the experiments for this study. In section 3 we analyse which of the three time scales that we have presented fit the observed time scale of the experiments. Finally, in section 4 we discuss our results and compare with other studies.

2. Model setup and experiments

We have performed an experiment in which we perturb the density field of an OGCM at high northern latitude, and we have investigated which of the time scales described in the previous section dominate the response at high southern latitude. For this we have used the recently developed and purely Python based ocean general circulation model VEROS (Häfner et al., 2018). The advantage of using VEROS is that ocean experiments can be prepared in very little time without compromising the physics of a GCM. This has allowed us to rapidly investigate a number of experiments in this paper. Combined with matrix fusion algorithms, this Python code is about 50% slower than comparable Fortran codes, but this is more than compensated by its ease of use, and the fact that the simulations can be performed using GPUs.

Our setup is similar to the idealized Atlantic slice setup of Munday et al. (2013) (see Fig. 3). The model domain spans from 60°S to 60°N, and 30° in longitude. The depth of the basin is 4000 m, but with a sill depth of 2000 m located south of 40°S. The sill gives rise to periodic boundary conditions in the upper half of the southern part of the domain, and the setup is therefore a combination of both a basin and a (periodic) channel. This is to mimic the Atlantic basin together with Drake Passage and the SO, and we will also term the northern part of the basin the North Atlantic (NA), the southern part of the basin will be termed the South Atlantic (SA), and the channel will be termed the Southern Ocean (SO). The parameters used can be found in Table 1. The forcing applied to the model can be seen in Fig. 3: The upper surface is forced by a zonal wind stress given by

$$F_x(\theta) = \begin{cases} F_{\mathrm{SO}} \sin\left(\pi \frac{\theta+60^\circ}{30^\circ}\right), & \text{if } \theta < -30^\circ \\ -F_{\mathrm{B}} \sin\left(\pi \frac{\theta+30^\circ}{30^\circ}\right), & \text{if } -30^\circ < \theta < -5^\circ \\ -F_{\mathrm{EQ}} \left(1.5 \cos\left(\pi \frac{\theta-10^\circ}{10^\circ}\right) + 2.5\right), & \text{if } -5^\circ < \theta < 5^\circ \\ F_{\mathrm{B}} \sin\left(\pi \frac{\theta-30^\circ}{30^\circ}\right), & \text{if } 5^\circ < \theta < 30^\circ \\ -F_{\mathrm{B}} \sin\left(\pi \frac{\theta-60^\circ}{30^\circ}\right), & \text{if } 30^\circ < \theta \end{cases} \tag{6}$$

where $F_{\mathrm{SO}} = 0.15\,\mathrm{N/m^{-2}}$, $F_{\mathrm{B}} = 0.05\,\mathrm{N/m^{-2}}$ and $F_{\mathrm{EQ}} = 0.01\,\mathrm{N/m^{-2}}$. This is in idealisation if the actual winds in the Atlantic basin and the SO, with strong winds in the SO and gyre-inducing wind forcing in the Atlantic.

The surface is relaxed to a temperature profile given by

$$T^*(\theta) = \begin{cases} T_s + \Delta T \sin\left(\pi \frac{\theta+60^\circ}{120^\circ}\right), & \text{if } \theta < 0^\circ \\ T_n + (\Delta T + T_s - T_n) \sin\left(\pi \frac{\theta+60^\circ}{120^\circ}\right), & \text{if } 0^\circ < \theta, \end{cases} \tag{7}$$

with $T_s = 0\,^\circ\mathrm{C}$, $T_n = 5\,^\circ\mathrm{C}$ and $\Delta T = 25\,^\circ\mathrm{C}$. The relaxation constant is found in Table 1. The north-south asymmetry with 5°C higher temperatures in the North is used to mimic the temperature difference between the areas of deep convection in the North Atlantic and the southern most part of the SO. No salinity forcing is included until a fresh water perturbation is applied, so the salinity is initially everywhere $S_n = 35$ PSU.

Our standard setup was configured with the parameters from Table 1 and the initial simulation was spun up for 1000 years. The isopycnal diffusivity (diffusion along isopycnals, Redi (1982)) is set equal to κ_{GM}, but since we have used temperature as the only density controlling tracer, we have effectively removed the effect of isopycnal diffusion, since there is no longer any temperature gradient along density gradients. This means that the only eddy processes which have an impact on the simulation are those of the GM-advection.

After the initial spin-up, the model was branched into five ensemble members each differing from the original configuration by a single model parameter. That is either κ_{GM}, K_{v} or f_{s} was modified. Each member of this small ensemble of simulations was integrated for another 500 years. The description of the ensemble members is found in Table 2.

Parameter	**Symbol**	**Value**	**Units**
Horizontal viscosity	ν_h	10^5	m^2/s
Time step	Δt	3600	s
Salt restoring timescale	τ_S	30	days
Temperature restoring timescale	τ_T	10	days
Eddy transfer coefficient*	κ_GM	1000	m^2/s
Background vertical diffusivity*	K_v	$2 \cdot 10^{-5}$	m^2/s
Horizontal resolution*	-	2 degrees	$^\circ$
Vertical resolution varies by:	10m (top)	250m (bottom)	40 layers
Surface area	A	$3 \cdot 10^{13}$	m^2

Table 1: Model parameters used in the standard configuration (The * means that parameter varies in the different experiments)

Symbol	Value	Description
$\kappa_{1/2}$	$500\,\mathrm{m}^2/\mathrm{s}$	Uses half the value of κ_GM
κ_2	$2000\,\mathrm{m}^2/\mathrm{s}$	Uses double the value of κ_GM
$K_{1/2}$	$1 \cdot 10^{-5}\,\mathrm{m}^2/\mathrm{s}$	Uses half the value of K_v
K_2	$4 \cdot 10^{-5}\,\mathrm{m}^2/\mathrm{s}$	Uses double the value of K_v
$f_{1/2}$	Varies with latitude	Uses half the Coriolis parameter

Table 2: Description of the enemble of branch runs of our model simulations. The model parameters for each ensemble member are the those from Table 1, but one parameter is changed as shown in this table. The span in κ_GM is chosen to mach the the span reported in Kuhlbrodt et al. (2012), and the span in K_V is to mimic the spread in upper ocean mixing reported by Waterhouse and Coauthors (2014)

After the spin-up we apply a fresh water perturbation inspired by Pedro et al. (2018) to all ensemble members. We do this be relaxing the surface ocean towards the following profile:

$$S^*(\theta) = \begin{cases} S_n, & \text{if } \theta < 50^\circ \\ S_n - 1\ \mathrm{PSU} \sin\left(\frac{-\pi}{2}\frac{50-\theta}{10^\circ}\right), & \text{if } 50^\circ < \theta, \end{cases} \tag{8}$$

where $S_n = 35$ PSU, and the relaxation time is found in Table 1. The perturbation is applied to lower the salinity and hence the density in northern most part of the NA. After applying the perturbation, the models were integrated for another 400 years The introduction of salinity differences also means that isopycnal diffusion will be present in the simulations, but within the integration time, only high latitude NA gained a salinity gradient. Perturbations with a northern salinity increase were also performed, but they gave the same result as the fresh water perturbation, and will not be discussed further.

3. Results

Based upon the scaling analysis here, the expectation is that the adjustments towards a new steady state will contain five parts (see Figure 2): (1) Boundary wave propagation, (2) geostrophic adjustments in the basin (3) Rossby wave propagation, (4) eddy transport in the SO and (5) diabatic uptake and diffusion of heat. We expect the propagation time of the waves to be short compared with the overall adjustments, but we don't know which of the remaining processes is the limiting factor for the time scale of adjustment in the SO.

The initial effects of the freshwater perturbation follows Kawase (1987) (see Figure 4) closely with a boundary wave running first at the western boundary in the NA, then along the equator followed by a a wave a the eastern boundary in the SA. Rossby waves are emitted from the eastern boundary wave. The crossing time of the waves is short as expected. In all simulations, the perturbation results in a reduced meridional overturning circulation. As a result, the northern part of the NA cools down, while the SA starts to warm slowly. The warming is largely confined by the isotherms as seen in Figure 5. The overall changes in thermal structure is similar to that found by Vettoretti and Peltier (2015) and Pedro et al. (2018).

In the SA, the warming begins approximately 1 - 2 years after the perturbation is applied (the flat initial part of Figure 6). The warming in the SA starts later the more southerly in latitudes we look. We interpret this as the time it takes for the boundary wave to reach a given latitude. Slower than the classical Kelvin wave, but in good agreement with Marshall and Johnson (2013), who show that the adjustments on longer timescales is accomplished by a Rossby-like boundary wave with phase speeds slightly smaller than Kelvin waves.

After the boundary wave has reached a given latitude, the adjustments generally show the behavior of a relaxation process, as seen in Figure 6. This means that for most positions, we can attribute an e-folding time scale for the adjustment to the new steady state temperature. We can also define the time it takes for the adjustment to be "nearly" complete, τ_{full}, as the time when the adjustment has reached the fraction $2/e$ of its final value. τ_{full} will generally be a function of space and the model parameters of Tables 1 and 2. When the isotherms of the SA deepen, the isotherms in the SO follow as one would expect from the thickness diffusion.

In the introduction we gave different suggestions on what sets $\tau_{\rm full}$: In the SA we expect $\tau_{\rm full}$ to be determined by either (a) $f_{\rm s}$ as in eq. 2, if the geostrophic adjustments are the limiting ones, or (b) by $K_{\rm V}$ as in eq. 4 if diabatic heat diffusion and uptake is the limiting factor. In the SO we expect $\tau_{\rm full}$ to be set by whatever process controls the basin adjustment AND eddy heat tranport - that is on $\kappa_{\rm GM}$ as in eq. 3 (Recall that $\tau_{\rm full}$ calculated in the SO is our representation of the BSTL). In the next set of subsections we investigate the mechanisms that set $\tau_{\rm full}$ in the SA.

3.1. Adjustments in the SA

First we focus on the mechanisms that operate at the edge of the channel (at 35°S). Table 3 shows how $\tau_{\rm full}$ and the e-folding time compare for the different experiments. We also show an estimate of the adjustment time calculated using eqs. 2 and 5 as we have assumed that eq. 2 is expected to be an e-folding time, and hence might compare directly to the e-folding time of the experiment.

Parameter varied	standard	$\kappa_{1/2}$	κ_2	$K_{1/2}$	K_2	$f_{1/2}$
Scaling estimates	28.5	27.9	29.3	31.6	24.7	15.5
e-folding time at 35°S (years)	28.5	25.8	29.1	35.8	25.1	17.2
$\tau_{\rm full}$ at 35°S (years)	70.1	63.2	65.9	85.6	63.5	39.9

Table 3: Adjustment times at 35°S read out from figures similar to Figure 6. To calculate the the scaling estimates we used eq. 5 and eq. 2 along with the values $g' = 0.014 m/s^2$, $L_{\rm s} = 10°$ and $F_{\rm SO} = 0.15\,{\rm N/m^{-2}}$. These values where used partially because they fit the model output, partially because they gave the right time scale for the standard configuration.

If the diabatic process of eq. 4 is dominant in setting $\tau_{\rm full}$, then $\tau_{\rm full}$ should vary inversely with $K_{\rm v}$. Clearly, this is not the case here. If the adiabatic and geostrophic process of eq. 2 are dominant in setting $\tau_{\rm full}$, then $\tau_{\rm full}$ should vary proportional to $f_{\rm s}$. This is indeed the case. Furthermore, $\tau_{\rm full}$ shows a weak dependency on $K_{\rm v}$ and $\kappa_{\rm GM}$. This can be accounted for by investigating the influence that these parameters have on setting H as in eq. 5: As shown in Table 3 a calculation of the adjustment time using eqs. 5 and 2 show good agreement with the actual e-folding time (recall that eq. 2 is supposed to provide an estimate on the e-folding time). So the vertical mixing, K_v, plays a role by setting H, but the diffusive time scale τ_diff of eq. 4 is not a limiting factor for the adjustment, because it is too fast.

3.2. Adjustments in the SO

We now have evidence that the adjustments of the SA is determined by the geostrophic and adiabatic adjustments of eq. 2. Since we expect the heat accumulating in the SO to originate from the basin, we expect this dependency to carry over to the adjustment time of the SO - but we also expect the SO adjustment time to depend on the efficiency of the eddy advection as suggested by eq. 3. To test this we calculate τ_full for 50°S - that is the sea ice edge in Pedro et al. (2018) - at a depth of 500 m. But we also calculate τ_cross - the difference between τ_full at 35°S and 50°S. Values can be found in Table 4.

Parameter varied	standard	$\kappa_{1/2}$	κ_2	$K_{1/2}$	K_2	$f_{1/2}$
τ_full at 50°S (years)	135	~ 165	89.6	145	122	102
τ_cross	64.9	~ 102	26.4	59.4	58.5	68.4

Table 4: Adjustment times at 50°S read out from figures similar to Figure 6.

From Table 4 we see that τ_full in the SO has a dependency on f_s, but it is not a proportionality and hence doesn't resemble eq. 2 as clearly as was the case in the SA. This can be explained by the contribution from eddy advection: τ_cross shows the inverse dependency on κ_GM we could expect from eq 3, and no clear dependency on other parameters. These parameter dependencies confirm our intuition that eddy advection mainly carries the signal across the ACC. Therefore, in the SO τ_full is the sum of two parts: The adjustment time in the SA plus the time it takes eddies to bring the signal across the ACC. Therefore, we conclude that the time it takes the polar Southern Ocean to come to a new equilibrium after the AMOC has collapsed is, in this model, determined in roughly equal parts by advection in the SA, and eddy fluxes in the SO.

4. Discussion

We have investigated how different oceanic processes affect the time it takes the high southern latitudes to adjust to changes occurring at a high northern latitudes using an OGCM with an idealized setup of the Atlantic basin and the Southern Ocean.

Kawase (1987) showed that adjustments within ocean basins are mediated through planetary waves. The adjustments seen in the SA in our experiments are, however, far too slow to be set by the propagation speed of waves. Instead the adjustment time is set by the geostrophic process described in the introduction, into which the waves are embedded (Johnson and Marhsall (2002)). The importance of these adjustments for the BSTL has been suggested already by Schmittner et al. (2003).

The complete adjustment time between the northern high-latitude initial signal and the Antarctic coast is composed of the SA adjustment time plus the time it takes eddies to transport the heat into the SO. Interestingly it turns out that for a high values of κ_{GM} the adiabatic adjustments in the SA constitutes the main part of the SO adjustment time and hence possibly the BSTL.

Since our ocean basin has only about 1/3 (Table 1) the area of the real Atlantic, then according to eq. 2, the basin adjustment time could be three times slower than estimated here. This suggests that the main part of the adjustments in SO is determined by processes that occurs in the SA. This may be the reason why it is not possible to detect a difference between the time lag in the $\kappa_{\mathrm{GM}} = 3000\mathrm{m}^2/\mathrm{s}$ and $\kappa_{\mathrm{GM}} = 4000\mathrm{m}^2/\mathrm{s}$ full ESM runs shown in Figure 1. For realistic Atlantic basin sizes and a κ_{GM} not to small, the transport in the Southern Ocean is not a limiting factor for the overall adjustment. Indications of this was found by Vettoretti and Peltier (2015) who find that in a full ESM the signals in the SA and at Antarctica are similar.

How to compare our adjustment time scale - τ_{full} - to the BSTL of Svensson (2020) is not obvious. They have the same order of magnitude, but they have different meanings: Our time scale is an adjustment time scale - a continuous relaxation process that initiates as soon as the boundary wave has reached the southern border of the Atlantic basin. Svensson (2020)'s bipolar volcanic based synchronization is a time lag - the point where the Antarctic temperature starts to drop.

As Pedro et al. (2018) has suggested other mechanisms are needed to move the signal further south onto the Antarctic continent: melting of sea ice from below by the warm anomalies acquired from the oceanic adjustments. Sea ice is particularly exposed to heating from below, and melting of sea ice is a fast process (Bitz and Polvani (2012)). We further suggest that this is what might turn our relaxation signal into a time lag: The melting of sea ice acts as barrier that can only be overcome when heat has accumulated to a certain threshold.

The good agreement between the BSTL seen in Figure 1 and that obtained from Svensson (2020) indicates that the processes controlling the BSTL is well resolved within current climate models. We also note that the ocean processes described here are unlikely to work in reverse (i.e., a change in AABW production will not trigger a Kelvin wave at thermocline depth along the South American shelf). Therefore, we propose to refer at least to the oceanic component of the bipolar seesaw as the Greenland clipper and replace the mental image of a slow, reversible process with a fast irreversible one.

4.1. Acknowledgements:

This work is partially based on LSA's master thesis work in the TeamOcean group at University of Copenhagen (UCph). LSA and AvdH have carried out part of this work under the program of the Netherlands Earth System Science Centre (NESSC), financially supported by the Ministry of Education, Culture and Science (OCW). This project (LSA) has received funding from the European Unions Horizon 2020 research and innovation programme under the Marie Skodowska- Curie, grant agreement No 847504. Computational resources where provided by the Danish Center for Climate Computing (DC3), UCph and UU. Also a special thanks to Dion Häfner for helping with the VEROS simulations.

References

Allison, L. C., H. L. Johnson, and D. P. Marshall
2011. Spin-up and adjustment of the Antarctic Circumpolar Current and global pycnocline. *Journal of Marine Research*, 69:167–189.

Barker, S. and P. Diz
2014. Timing of the descent into the last Ice Age determined by the bipolar seesaw. *Paleoceanography*, 29:489–507.

Bitz, C. M. and L. M. Polvani
2012. Antarctic climate response to stratospheric ozone depletion in a fine resolution ocean climate model. *Geophysical Research Letters*, 39:1–5.

Broecker, W. S.
1998. Paleocean circulation during the last deglaciation: A bipolar seesaw? *Paleoceanography*, 13:119–121.

Buizert, C., M. Sigl, M. Severi, B. R. Markle, J. J. Wettstein, J. R. McConnell, J. B. Pedro, H. Sodemann, K. Goto-Azuma, K. Kawamura, S. Fujita, H. Motoyama, M. Hirabayashi, R. Uemura, B. Stenni, F. Parrenin, F. He, T. J. Fudge, and E. J. Steig
2018. Abrupt ice-age shifts in southern westerly winds and Antarctic climate forced from the north. *Nature*, 563:681–685.

Gent, P. and J. Mcwilliams
1990. Isopycnal Mixing in Ocean Circulation Models. *Journal of Physical Oceanography*, 20:150–155.

Gent, P., J. Willebrand, T. McDougall, and J. McWilliams
1995. Parameterizing Eddy-Induced Tracer Transports in Ocean Circulation Models. *Journal of Physical Oceanography*, 25:463–474.

Gnanadesikan, A.
1999. A Simple Predictive Model for the Structure of the Oceanic Pycnocline. *Science*, 283:2077–2079.

Griffies, S. M.
2003. *Fundamentals of Ocean Climate Models*, Pp. 221–226,289–292.

Häfner, D., R. L. Jacobsen, C. Eden, M. R. Kristensen, M. Jochum, R. Nuterman, and B. Vinter
2018. Veros v0.1 - A fast and versatile ocean simulator in pure Python. *Geoscientific Model Development*, 11:3299–3312.

Jochum, M. and C. Eden
2015. The Connection between Southern Ocean Winds, the Atlantic Meridional Overturning Circulation, and Indo-Pacific Upwelling. *Journal of Climate*, 18:9250 – 9257.

Johnson, H. and D. Marhsall
2002. A Theory for the Surface Atlantic Response to Thermohaline Variability. *Journal of Physical OCeanography*, 32:1121–1132.

Kawase, M.
1987. Establishment of Deep Ocean Circulation Driven by Deep-Water Production. *J. Phys. Oceanogr.*,, 17:2294–2317.

Kuhlbrodt, T., R. S. Smith, Z. Wang, and J. M. Gregory
2012. The influence of eddy parameterizations on the transport of the Antarctic Circumpolar Current in coupled climate models. *Ocean Modelling*, 52-53:1–8.

Lacasce, J. H. and J. Pedlosky
2004. The Instability of Rossby Basin Modes and the Oceanic Eddy Field. *Journal of Physical Oceanography*, 34:2027–2041.

Ledwell, J. R., A. J. Watson, and C. S. Law
1993. Evidence for slow mixing across the pycnocline from an open-ocean tracer-release experiment. *Nature*, 364:701–703.

Li, C. and A. Born
2019. Coupled atmosphere-ice-ocean dynamics in Dansgaard-Oeschger events. *Quaternary Science Reviews*, 203:1–20.

Marshall, D. P. and H. L. Johnson
2013. Propagation of meridional circulation anomalies along western and eastern boundaries. *Journal of Physical Oceanography*, 43:2699–2717.

McWilliams, J. C.
2006. Fundamentals of Geophysical Fluid Dynamics. Pp. 161–163,209–212.

MorenoChamarro, E., D. Ferreira, and J. Marhsall
2020. Polar Phasing and CrossEquatorial Heat Transfer Following a Simulated Abrupt NH Warming of a Glacial Climate. *Paleoceanography and Paleoclimatology*, 35.

Munday, D. R., H. L. Johnson, and D. P. Marshall
2013. Eddy saturation of equilibrated circumpolar currents. *Journal of Physical Oceanography*, 43:507–532.

Nielsen, S. B., M. Jochum, J. B. Pedro, C. Eden, and R. Nuterman
2019. Two-Timescale Carbon Cycle Response to an AMOC Collapse. *Paleoceanography and Paleoclimatology*, 34:511–523.

Nikurashin, M. and G. Vallis
2011. A theory of deep stratification and overturning circulation in the ocean. *Journal of Physical Oceanography*, 41:485–502.

Pedro, J. B., M. Jochum, C. Buizert, F. He, S. Barker, and S. O. Rasmussen
2018. Beyond the bipolar seesaw: Toward a process understanding of interhemispheric coupling. *Quaternary Science Reviews*, 198:27–46.

Peltier, W. R. and G. Vettoretti
2014. Dansgaard-Oeschger oscillations predicted in a comprehensive model of glacial climate: A "kicked" salt oscillator in the Atlantic. *Geophysical Research Letters*, 41:7306–7313.

Poulsen, M. B., M. Jochum, and R. Nuterman
2018. Parameterized and resolved Southern Ocean eddy compensation. *Ocean Modelling*, 124:1–15.

Redi, M.
1982. Oceanic Isopycnal Mixing by Coordinate Rotation. *Journal of Physical Oceanography*, 12:1154–1158.

Samelson, R. M.
2011. Time-Dependent Adjustment in a Simple Model of the Mid-Depth Meridional Overturning Cell. *Journal of Physical Oceanography*, 41:1009–1025.

Schmittner, A., O. A. Saenko, and A. J. Weaver
2003. Coupling of the hemispheres in observations and simulations of glacial climate change. *Quaternary Science Reviews*, 22:659–671.

Stocker, T. F. and S. J. Johnsen
2003. A minimum thermodynamic model for the bipolar seesaw. *Paleoceanography*, 18:1–11.

Svensson, A. C.
2020. Bipolar volcanic synchronization of abrupt climate change in Greenland and Antarctic ice cores during the last glacial period. *Climate of the Past*, 16:1565–1580.

Vallis, G. K.
2017. *Atmospheric and oceanic fluid dynamics: Fundamentals and large-scale circulation, second edition*, Pp. 853–858.

Vettoretti, G. and P. Peltier
2015. Interhemispheric air temperature phase relationships in the nonlinear Dansgaard-Oeschger oscillation. *Geophysical Research Letters*, 42:1180–1189.

Vettoretti, G. and W. R. Peltier
2018. Fast Physics and Slow Physics in the Nonlinear DansgaardOeschger Relaxation Oscillation. *Journal of Climate*, 31:3423–3449.

Viebahn, J., A. von der Heuydt, D. Le Bars, and H. Dijkstra
2016. Effects of Drake Passage on a strongly eddying global ocean. *Pale-oceanography*, 31:564–581.

WAIS Divide Project Members
2015. Precise interpolar phasing of abrupt climate change during the last ice age. *Nature*, 520:661–665.

Waterhouse, A. and Coauthors
2014. Global Patterns of Diapycnal Mixing from Measurements of the Turbulent Dissipation Rate. *Journal of Physical Oceanography*, 44:1854–1872.

Weaver, A. J. and Sarachik
1990. On the Importance of Vertical Resolution in Certain Ocean General Circulation Models. *Journal of Physical Oceanography*, 20:600–609.

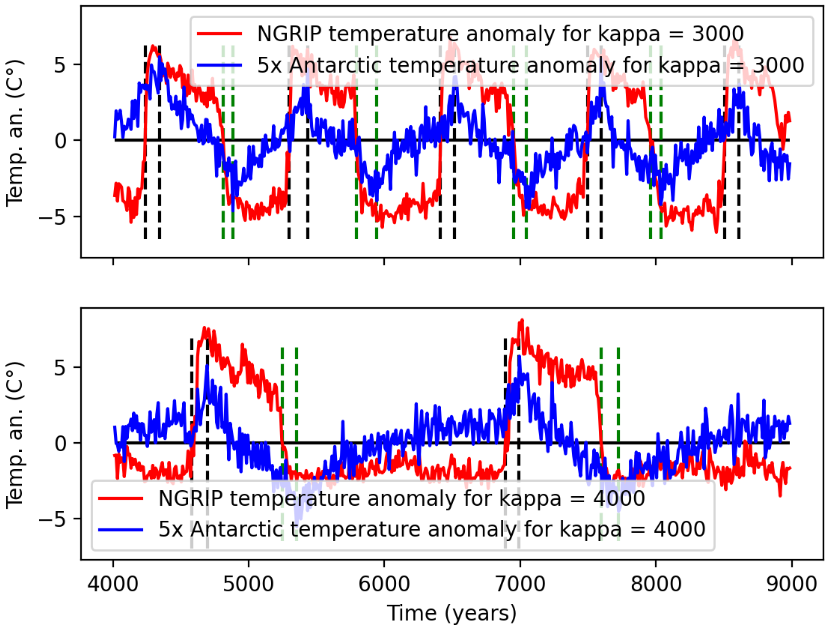

Figure 1: Greenland and (5x) Antarctic temperature anomaly (mean subtracted) from a low-resolution glacial simulation of the DO oscillation using CESM1 (Vettoretti and Peltier (2018)) for two different values of κ_{GM}. The time lag between initiation/termination of interstadials and their Antarctic counterpart is $\sim$ 100 years - both for (upper panel) $\kappa_{\mathrm{GM}} = 3000\mathrm{m}^2/\mathrm{s}$ and (lower panel) $\kappa_{\mathrm{GM}} = 4000\mathrm{m}^2/\mathrm{s}$. Notice that these are nominal values used for horizontal diffusivity in the surface. The subsurface values for thickness diffusion in the Southern Ocean are approximately a factor 4 smaller (Jochum and Eden (2015)). The time lag is indicated by the vertical lines, with black lines indicating initation of interstadials, and green lines indicating termination. For the lag we have used the definition from Svensson (2020).

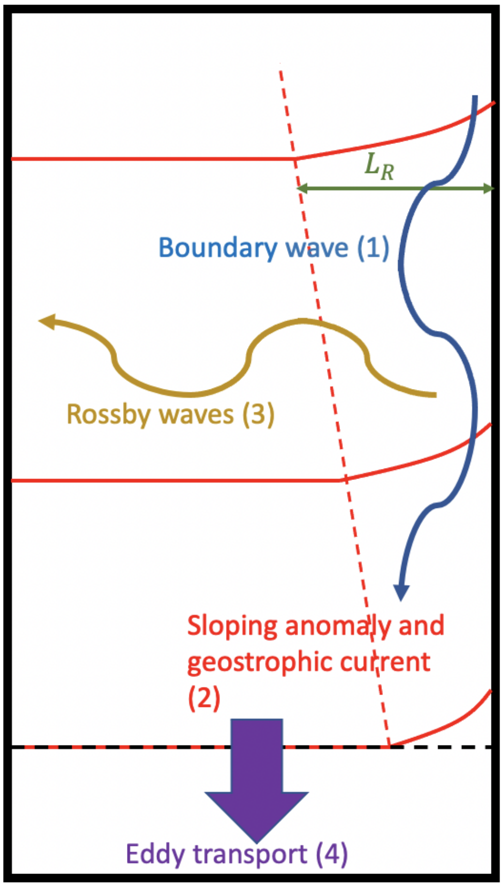

Figure 2: A summary of the adiabatic processes involved in the adjustment in the South Atlantic and Southern Ocean. (1) A boundary wave travels southward from equator. (2) Due to changing Rossby radius, L_r, part of the wave scatters into a geostrophic current at the eastern boundary. (3) The slope supporting the geostrophic current radiates into the interior of the South Atlantic. (4) Southern Ocean eddies advect the signal across the ACC. On top of this there are (5) diabatic adjustments. This figure is inspired by McWilliams (2006).

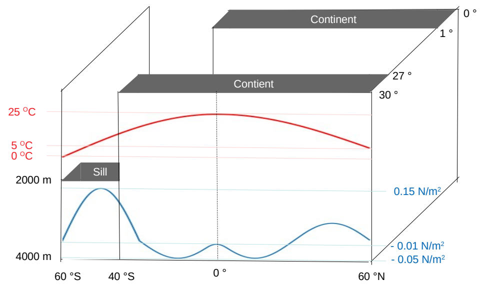

Figure 3: The model consists of a basin that spans the latitudes from 40°S to 60°N, and a periodic channel in the southern part. The channel has a sill to resemble the Drake Passage. The wind stress profile is shown in blue, and the temperature relaxation is shown in red

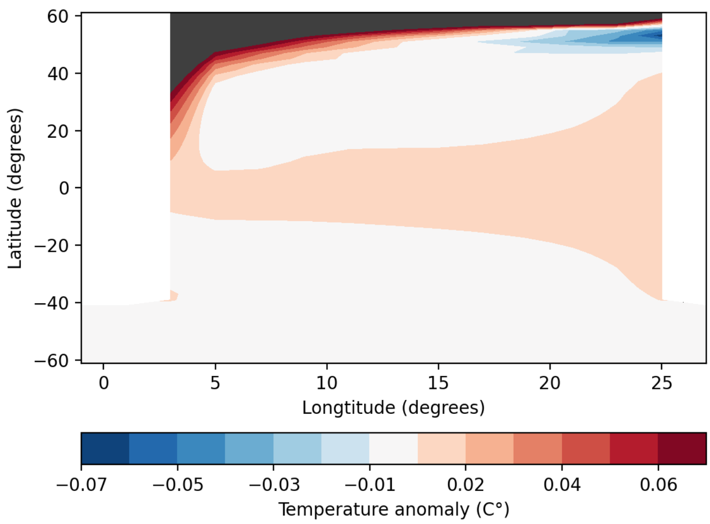

Figure 4: Temperature anomaly at 500 m depth after 3 years. The boundary waves and the equatorial kelvin wave are easy to identify. The cold pool in the NA is located where heat is no longer delivered by the overturning.

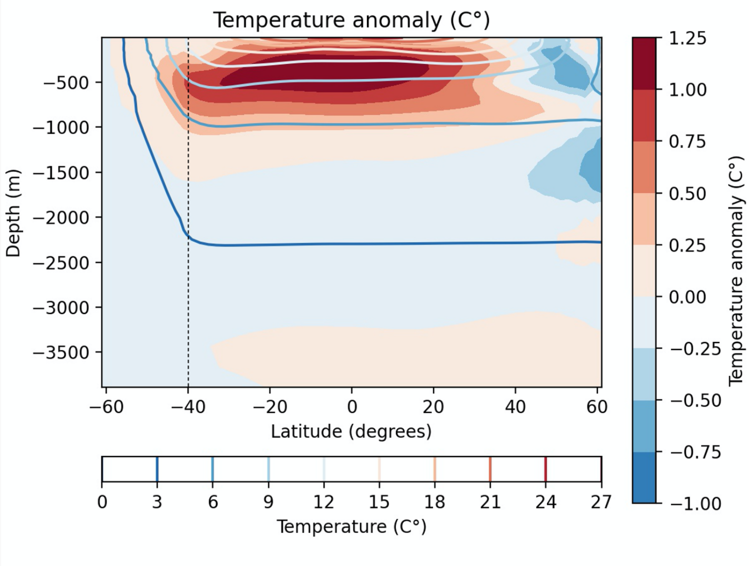

Figure 5: Temperature anomaly after 400 years for the standard configuration. The temperature drops in the sinking regions of the NA, and in SA and SO, the heating pattern is confined by isopycnals. This is similar for all experiments, and should be similar to the coupled modelling results from Vettoretti and Peltier (2015) and Pedro et al. (2018). The open contour lines correspond to the initial position of the isoterms.

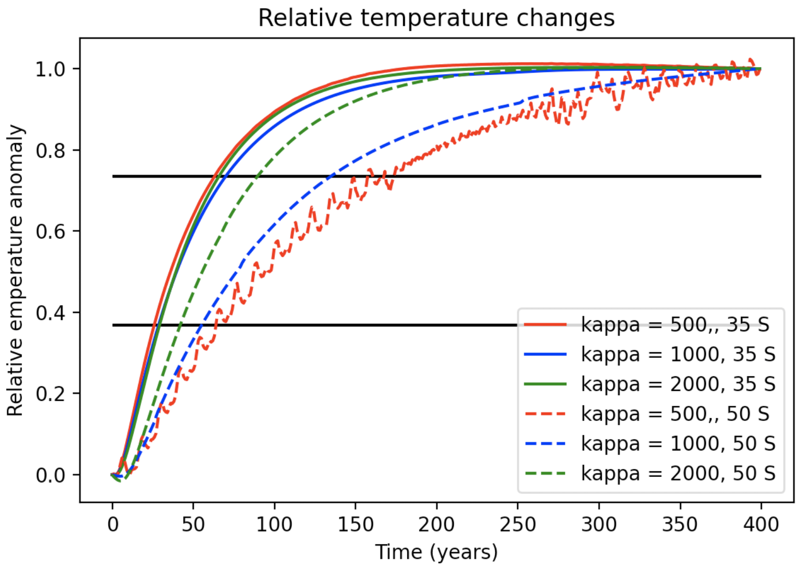

Figure 6: Relative changes in temperature as a function of time for the different values κ_{GM} for 35°S (solid lines) and 50°S (dashed lines). The two black lines correspond to $1/e$ and $2/e$, and are used to read of the e-folding time and τ_{full}. Notice that the higher κ_{GM} is the more similar the adjustment at the two locations. This stems from the faster eddy transport with a higher κ_{GM}. At 50°S the $\kappa_{1/2}$ fluctuations stem from numerical noise induced by too low diffusion for the given resolution (Weaver and Sarachik (1990)).

A.2 MODELLED NGRIP AND EDML TEMPERATURE TIME SERIES

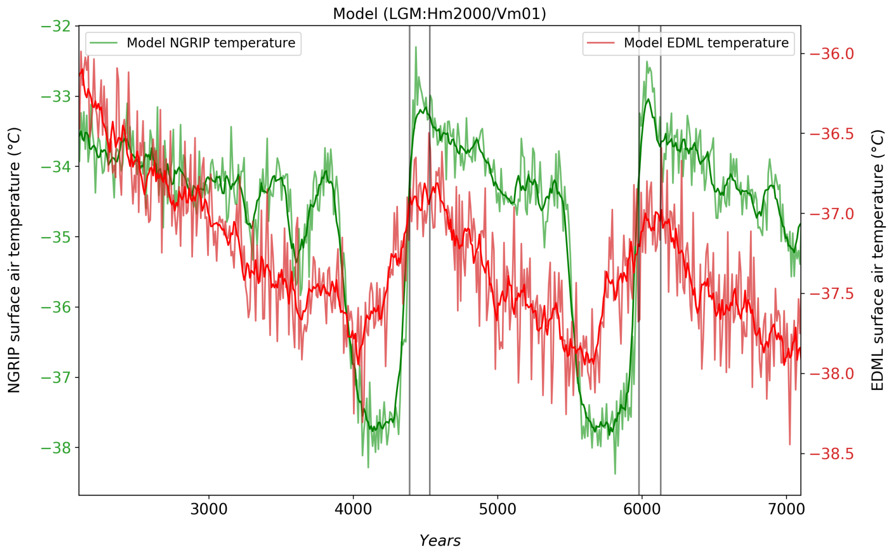

Figure 24: Surface temperature time series from the NGRIP and EDML location in the coupled model. The vertical lines marks the modelled DO onsets and the AIM events, the time-lag between them are 140 ± 10 yrs (first cycle) and 150 ± 10 yrs (second cycle).

A.3 TEMPERATURE ANOMALIES AT 1000 M DEPTH IN THE SOUTHERN OCEAN

Fig. 19 represented the temperature anomalies at 1000 m depth around the timing of the second warming event produced by the LGM experiment in CESM1, in addition to that, the changes occurring around the first stadial is presented here.

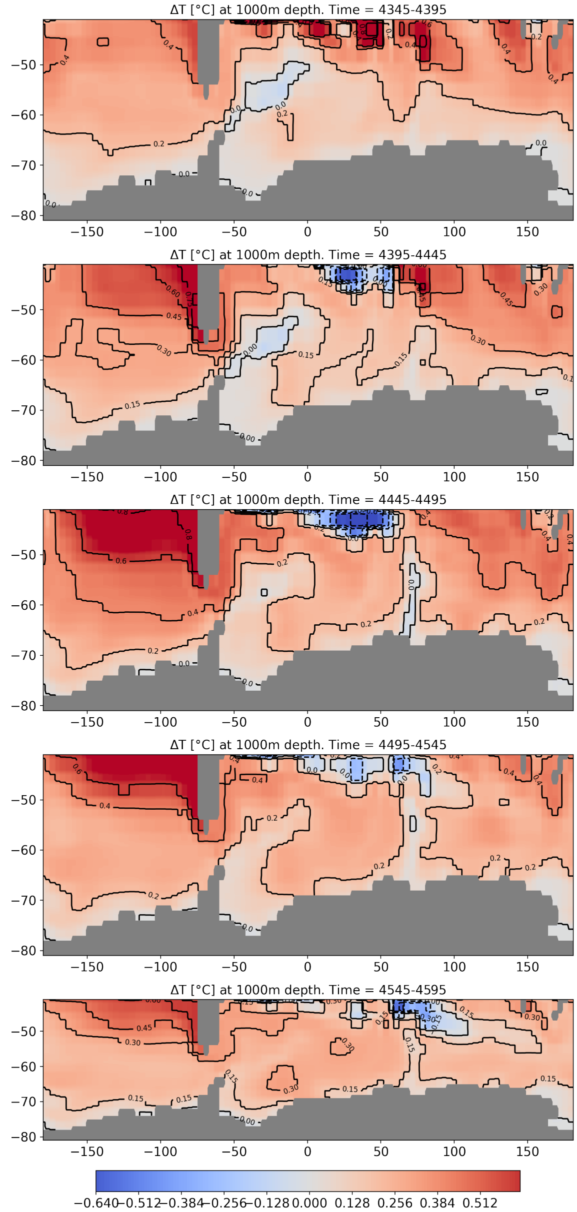

Figure 25: A temperature anomaly map of the Southern Ocean at fixed depth at 1000 m below the surface and its numbered contour lines are plotted along it. Each subplot is presenting the average temperature anomaly between the prescribed time range of 50 years. These temporal changes are visualizing the environments due to the first interstadial signal produced by the LGM experiment in CESM1.